İSTANBUL TECHNICAL UNIVERSITY ★ INSTITUTE OF SCIENCE AND TECHNOLOGY

INCREASING OF FATIGUE STRENGTH AND CORROSION RESISTANCE OF QUENCHED AND TEMPERED STEELS BY CONTROLLED GAS NITRIDING

M.Sc. Thesis by
Zühre VAROL

Department : Advance Tecnology Department

Programme : Material Science and Engineering

JUNE 2011

İSTANBUL TECHNICAL UNIVERSITY ★ INSTITUTE OF SCIENCE AND TECHNOLOGY

INCREASING OF FATIGUE STRENGTH AND CORROSION RESISTANCE OF QUENCHED AND TEMPERED STEELS BY CONTROLLED GAS NITRIDING

M.Sc. Thesis by
Zühre VAROL
(521091035)

Date of submission : 04 May 2011
Date of defence examination: 10 June 2011

Supervisor (Chairman) : Prof. Dr. Mustafa ÜRGEN (ITU)
Members of the Examining Committee : Prof. Dr. Müzeyyen MARŞOĞLU (YTU)
Assis. Prof. Dr. Kürşat KAZMANLI (ITU)

JUNE 2011

İSTANBUL TEKNİK ÜNİVERSİTESİ ★ FEN BİLİMLERİ ENSTİTÜSÜ

KONTROLLÜ GAS NİTRÜRLEME İLE SERTLEŞTİRİLMİŞ ÇELİKLERİN YORULMA VE KOROZYON DİRENCİNİN ARTTIRILMASI

YÜKSEK LİSANS TEZİ
Zühre VAROL
(521091035)

Tezin Enstitüye Verildiği Tarih : 04 Mayıs 2011
Tezin Savunulduğu Tarih : 10 Haziran 2011

Tez Danışmanı : Prof. Dr. Mustafa ÜRGEN (İTÜ)
Diğer Jüri Üyeleri : Prof. Dr. Müzeyyen MARŞOĞLU (YTÜ)
Doç. Dr. Kürşat KAZMANLI (İTÜ)

HAZİRAN 2011

FOREWORD

I would like to express my deep appreciation and thanks for my advisor Prof. Dr. Mustafa Ürgen in ITU and for my advisors Bülent Öklü and Dr. Nils Lippmann in Robert Bosch Turkey which this work is supported by. I would like to thanks also to my parents because of their supports along my all education life.

June 2011

Zühre VAROL

Chemical Engineer

TABLE OF CONTENTS

Page

ABBREVIATIONS

DI	**:** Diesel Injector
DS	**:** Diesel System
RBTR	**:** Robert Bosch Turkey
CR-Injector	**:** Common Rail Injector
HPC	**:** High Pressure Connector
KN	**:** Nitriding Potential
CL	**:** Compound Layer
DL	**:** Diffusion Layer
OM	**:** Optical Microscope
SEM	**:** Scanning Electron Microscope
GDOES	**:** Glow Discharge Optical Emission Spectroscopy
XRD	**:** X-Ray Diffraction
THS	**:** Through Hole Sample

LIST OF TABLES

Page

LIST OF FIGURES

Page

INCREASING OF FATIGUE STRENGTH AND CORROSION RESISTANCE OF QUENCHED AND TEMPERED STEELS BY CONTROLLED GAS NITRIDING

SUMMARY

By increasing importance of energy efficiency and CO_2 emision reduction, combustion of fuel is getting important in automative industry. Injectors should be resisted to high pressure levels to improve combustion and vaporization of fuel. Presently day, induction hardening is applied to get fatigue strength up to 1800-2000 bar but these pressure levels should be increase to 2500 bar and over. At the same time, corrosion should be prevented which occurs at the time of combustion and transportation. Therefore, sensor controlled gas nitriding process was developed to increase both fatigue strength and corrosion resistance for diesel injector components.

Two different material and three different componenets were used in the experimental matrix. These are 42CrMo4 and 50CrMo4. High pressure connector, Common Rail injector and trought hole sample were used as a components. The real componenets were used such a high pressure connector and CR-Injector because pressure pulsation test can be only proceed by real componenets. Therefore, high pressure connector which the material composition is 42CrMo4, was used for the first trial series which has similar geometry to CR-Injectors and is simpler than CR-Injector and also has low cost. CR-Injector was used for the second trial series which the material composition is 50CrMo4. After getting improvement with HPC and CR-Injector, pre-oxidation, nitriding and post-oxidation treatments were determined with trought hole samples which is similar to CR-Injector and 50CrMo4 material compositon to increase corrosion resistance.

2460 bar permitted pressure level was achived for the first trial series. Fracture analysis showed that components were failed from filter cartridge point. Investigation of compound layer thickness and its homogenity showed neccessarity of pretreatment before nitriding to activate specimen surface. And also neccesarity of improvement of corrosion resistance was seen in the salt spray test.

Permitted pressure level was calculated as 2550 bar for CR-Injectors in the second trial series. Trial with CR-Injector which was proceed at 520°C 1 hour uncontrolled nitriding and 5 hours controlled nitriding with K_N 0,40 had to been repeated because fuel discharge tube was closed at the nitriding process because of two directional nitriding. This place was closed by stop off coating and was nitrided again and pressure pulsation test was repeated. At the fracture analysis which was investigated for repeated pressure pulsation test, failure points were defined at thread, seal surfaces and hole diameter decreasing neccessarity of homogeneous compound layer and corrosion resistance were defined like HPC.

After getting improvement on fatigue strenght, four different pre-oxidation treatment parameters with air were defined with trought hole samples to homogenize compound layer thickness and also one trial was determined without pre-oxidation to compare with others. Three different post-oxidation treatments were determined to improve corrosion resistance. Trought hole samples were designed for third trail series because pressure pulsation test were not planned for pre and post oxidation investigation and also samples has low cost. Metalographic investigation were done for homogenization of compound layer. GDOES were used to investigate elemental analysis of compound layer. Corrosion tests were done by salt spray test for 5,5 hours. The best homogenization was achieved by pre-oxidation with 450°C - 1 hour. The fatigue strength was achieved by nitriding 520°C and 6 hours. The best corrosion resistance was achived by post-oxidation with 450°C-1 hour.

KONTROLLÜ GAS NİTRÜRLEME İLE SERTLEŞTİRİLMİŞ ÇELİKLERİN YORULMA VE KOROZYON DİRENCİNİN ARTTIRILMASI

ÖZET

Yakıt verimliliği ve CO_2 emisyon değerlerindeki düşüşün öneminin artmasıyla birlikte otomotiv endüstrisinde yakıtın yanmasının önemi daha da artmaktadır. Yakıtın daha iyi yanması ve dolayısıyla buharlaşmasının daha iyi olması için enjektörlerin daha yüksek basınçlara dayanıklı olması gerekmektedir. Günümüzde indiksiyonla sertleştirme ile elde edilen 1800-2000 bar basınçlar yerini 2500 bar ve üstü basınçlara bırakacaktır. Bunun yanında enjektörlerde yanma sırasında yüksek sıcaklıkla oluşan nemin ve enjektörlerin taşınma sırasında oluşabilecek korozyonun da engellenmesi gerekmektedir. Bu nedenle hem yüksek yorulma direnci hem de korozyon dayanımı sağlayabilecek, sensör kontrollü gaz nitrürleme prosesi dizel enjektör komponentleri için geliştirilmiştir.

Deneysel çalışmada 2 farklı malzeme ve 3 farklı komponent kullanılmıştır. Malzemeler 42CrMo4 ve 50CrMo4 dür. Komponent olarak; yüksek basınç bağlantı parçası, Common Rail (CR) enjector ve enjentör boyutlarına benzer örnek borular kullanılmıştır. Gerçek dizel enjektör komponentlerinin kullanılmasının nedeni yorulma dayanımı testinin (pulstest) gerçek komponenetler üzerinde yapılması gerektiğinden dolayıdır. Bu nedenle birinci deneme serisi CR enjektöre benzeyen, daha basit geometriye sahip ve maliyeti daha düşük olan 42CrMo4 malzemeden yapılmış yüksek basınç bağlantı parçası ile ikinci deneme serisi malzemesi 50CrMo4 olan CR enjektörler üzerinde yapılmıştır. Yorulma direncinde fark edilir bir artış sağlandıktan sonra korozyon dayanımının geliştirilmesi için tasarlanan ön oksidasyon, nitrürleme ve son oksidasyon proses adımları 50CrMo4 malzemeden yapılan örnek borular~~la~~ üzerinde gerçekleştirilmiştir.

Yapılan birinci seri denemeler sonrasında 2460 bar basınca ulaşılmıştır. Çatlak analizine bakıldığında parçaların pulstest sırasında monte edilen filtre birleşme noktasından çatladığı görülmüştür. Beyaz tabaka kalınlığına ve parça yüzeyindeki homojenliğine bakıldığında nitürleme öncesi yüzeyi temizleme amaçlı ön oksidasyon yapılabileceği ortaya çıkmıştır. Tuz püskürtme sis testi sonucunda korozyon dayanımın daha da iyileştirilmesi gerektiği ortaya çıkmıştır.

CR enjektörlerle yapılan ikinci seri denemeler sonucunda komponentin yorulma dayanımı 2550 bar çıkmıştır. 520°C'de yapılan pulstest, parçaların tamamının yakıt tahliye borusunun çift taraflı difüzyon sonucu kırılmasından dolayı test, yakıt tahliye borusunun ısıl işlem macunu ile kapatılıp tekrar nitrürlenmesiyle tekrar edilmiştir. İkinci pulstest sonucu yapılan çatlak analizinde komponenetlerin diş yüzeyi, yakut tahliye borusu çıkışı ve iç çap daralma noktası olduğu tespit edilmiştir. İlk deneme

serisinde olduğu gibi homojenizasyonun ve korozyon dayanımın iyileştirmesi gerektiği görülmüştür.

İlk iki deneme serilerinde basınç seviyelerinde artış gözlendikten sonra beyaz ve difüzyon tabakalarının parça yüzeyi boyunca homojenizasyonu için hava ile yapılan 4 farklı ön oksidasyon parametresi bir de karşılaştırma amaçlı ön oksidasyonsuz deneme planlanmıştır. Korozyon dayanımın Ri3 ve altı değerlerinin karşılaması için su ile yapılan 3 faklı son oksidayon parametresi tasarlanmış, pulstest yapılmayacağı için ve düşük maliyetli olması nedeniyle boyutları enjektöre benzer borular hazırlanmıştır. Yapılan üçüncü denem seri sonrası homojenizasyon için metalografik analiz yapılmıştır. Beyaz tabakanın elementel analizi için GDOES analizi yapılmıştır. Korozyon dayanımı testi 5,5 saatlik tuz püskürtme sis testi ile yapılmıştır. Üçüncü deneme serisin sonucunda en iyi homojenizasyon, istenen sertlik ile birlikte 450°C 1 saatlik parametre ile, en iyi yorulma direnci 520°C de 6 saat nitrürleme ile, en iyi korozyon dayanımı son oksidasyon parametresi olan 450°C 1 saat ile elde edilmiştir.

1. INTRODUCTION

Fuel injection technology represents one of the main drivers towards improving current characteristics of diesel engines and identifies future enhancements to reduce engine exhaust emissions (CO_2 emission), combustion noise and fuel consumption. In parallel to the continuously growing injection pressure, the number of injection events has been increased and the tolerances of the injected quantities has been reduced, a trend that will be followed in the future. By achieving the energy efficiency, there will be less CO_2 emmision which is shown below (Fig. 1.1). CO_2 emission reduction by fuel consumption for both gasoline and diesel technology. There need to be increase vaporization degree to achieve some performance with less fuel. Therefore, it is necessary to increase fatigue strength to resist high pressure levels to achieve high degree vaporization.

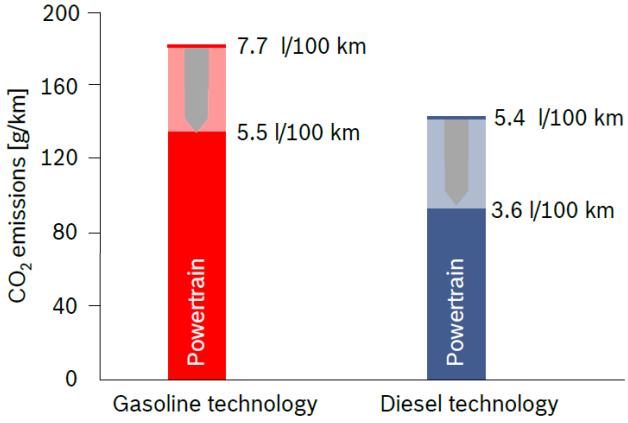

Figure 1.1 : CO_2 reduction in gasoline and diesel system by reduction of fuel [1]

Increasing demands on fuel efficiency and emission reduction require higher operating pressure and higher fatigue strength of the components. The actual applied heat treatment technologies (carburization, bainitization) for DI-components are not satisfying these requirements. Because of the absence of a quenching requirement with attendant volume changes, and the comparatively low temperatures employed in this process, nitriding of steels produces less distortion and deformation than either carburizing or conventional hardening. One of the potentials of the nitriding proses is

to get corrosion resistance with limited compound layer. Among the available nitriding processes (plasma, salt bath nitriding) gas nitriding is the most appropriate technique for our purpose since it allows nitriding of bores and holes. Moreover it is also possible to conduct gas nitriding at lower temperatures in a controlled manner. Therefore, within the scope of this work the development of the gas nitriding process for fuel injector parts is intended.

Gas nitriding of iron-based alloys is a very important surface engineering process and widely used in industry due to its beneficial influence on the fatigue behaviour and its improvement of the case resistance against wear and corrosion. However, the application practice is still largely based on phenomenology and experience. For this reason there is a great interest in scientific investigations of the processing methods in combination with control and predictability of materials properties.

Nitriding process is governed by the chemical potential of the saturating atmosphere, the kinetics of mass transfer,and the composition and structure of the surface layer of the parts. Controlled nitriding involves control ofthermodynamic and kinetic parameters and of surface activation process. Nitriding potential (K_N) is a ratio of partial pressure of ammonia and hydrogen in the gas phase atmosphere which involves chemical potential of nitrogen is the most important parameter in controlling the kinetics of nitriding process. In order to controlthe quality and obtain a nitrided layer with specified structure, it should be monitored and regulated.The values of K_N is determined in an in-situ mode using gas sensors. In-situ control of anitriding process with the sensorsis the most important tool for optimizing the structure of the layer and its quality.Today, control of the process of saturation on the basis ofthermodynamics with the use of special control of the saturatingmedium and the chemical potentials of nitrogen is possible only for the case of gas nitriding.

The aims of this thesis are the development of a sensor controlled gas nitriding process for Diesel injection components which are cyclic loaded to 2500 bar and additionaly investigate the possible usage of nitiriding for the improvement of the corrosion resistance on external surfaces of the parts. Post oxidaition of nitrided parts will also be investigated for the improvement of corrosion resistance without sacrifying the require fatique resistance.

2. GAS NITRIDING PROCESS

Nitriding is a thermochemical heat treatment process. Surface concentration of nitrogen, its state and process temperature are the key parameters that control the process. Therefore, to understand the effect of surface concentration of nitrogen, which is related to nitriding potential, temperature and time, thermodynamic and kinetics of the process must be well known.

2.1 Kinetics and Thermodynamics of Nitriding

2.1.1 Kinetics of nitriding

Gas nitriding is a case-hardening process whereby nitrogen is introduced into the surface of a solid ferrous alloy by holding the metal at a suitable temperature in contact with a nitrogenous gas, usually ammonia [2]. In the gas nitriding process, the steel is exposed to a carrier gas atmosphere with ammonia which decomposes to introduce nitrogen into the steel surface. The usualtemperature range is 490°C-580°C.

There are four steps of a gas nitriding process:

1. Reactions in the gas phase
2. Diffusion in the gas phase
3. Reactions at the steel surface
4. Diffusion into the steel

Step 1: Reactions in gas nitriding mainly involve the gases N_2, H_2, and NH_3.

Step 2: The gases which are dissociated and pure ammonia diffuse throught the gas atmosphere

Step 3: Reaction at the steel surface can be described as a genarally (Fig. 2.1):

$$NH_3 \Leftrightarrow \underline{N}_{\alpha-Fe} + \frac{3}{2}H_2 \qquad \textbf{(2.1)}$$

Step 4: Diffusion of nitrogen in steel has great influence on the nitriding rate.

In earlier calculations, it was normally assumed that diffusion in the steel is the only rate-determining step. To determine the rate of process, there should be selected the slowest stage of the process [3].

$$2NH_3 \rightarrow N_2 + 3H_2$$

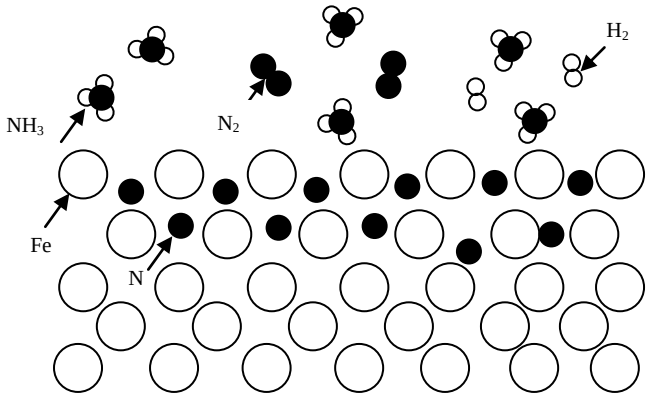

Figure 2.1 : Diffusion mechanism in gas nitriding process [4]

Gaseous nitriding involves a gas-metal reaction where the metallic sample is suspended in a furnace usually containing a flowing NH_3/H_2 gas mixture. Usually the nitrided surface region is subdivided into the compound layer adjacent to the surface, largely composed of iron nitrides, and the diffusion zone, where at the nitriding temperature the nitrogen is either dissolved (carbon steels) or precipitated as alloying element nitrides (Fig. 2.2).

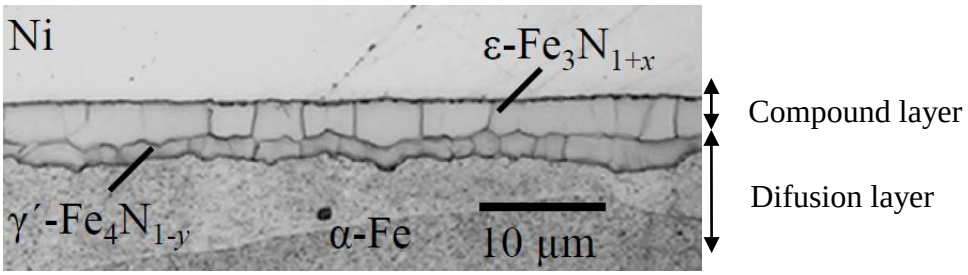

Figure 2.2 : Optical micrographs of compound-layer cross sections of gas nitrided α-Fe sheets after Nital etching [5]

Gas nitriding process has three different time dependent steps which are shown below (Fig. 2.3). These are heating step, nitriding step and cooling step. The main benefit of the nitriding is, it is not neccesary quenching because it proceeds below the austenite temperature.

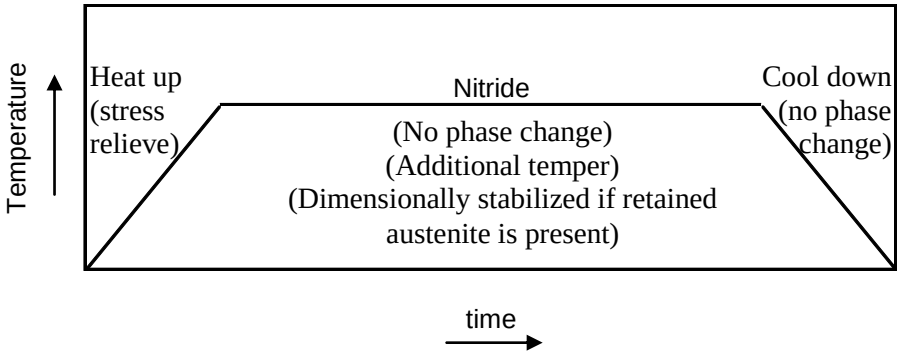

Figure 2.3 : Steps of the nitriding process [4]

i- Ammonia Dissociation Kinetics

An accurate description of the interaction of the NH_3 molecule with catalytically active surfaces is important to understand which factors determine the selectivity during catalytic reactions involving ammonia (Fig. 2.4). The elementary steps involved in the NH_3 adsorption and decomposition process are given below [6].

$NH_{3(g)} \rightleftarrows NH_{3ad}$ **(2.2)**

$NH_{3ad} \rightleftarrows NH_{2ad} + H_{ad}$ **(2.3)**

$NH_{2ad} \rightleftarrows NHa_{d} + H_{ad}$ **(2.4)**

$NH_{ad} \rightleftarrows N_{ad} + H_{ad}$ **(2.5)**

$2\ H_{ad} \rightarrow H_{2(g)}$ **(2.6)**

$2\ N(Hx)_{ad} \rightarrow N_{2(g)} + (x\ H_2)\ (x = 0, 1, 2, 3)$ **(2.7)**

ii- Diffusion Kinetics

The main reaction rate equation is writen below which represent reaction rate depends on temperature (T), activation energy (E_a), rate constant (k_0)

$$r_{nit} = k_0 \exp(\frac{-E_a}{RT}) f(R) f(\alpha) \quad \textbf{(2.8)}$$

Taking into account the surface reaction, the rate of the whole process can be expressed as follows:

$$r_{ads} - r_{des} = r_{solid\ phasereaction} + r_{dec} \quad \textbf{(2.9)}$$

r_{ads} = rate of the adsorption of a reactant from a gas phase,
r_{des} = rate of the desorption of an unreacted substrate from a solid surface,
$r_{solid\ phase\ reaction}$ = reaction in the solid state,
r_{dec} = recombination reaction of atomic species to form molecules

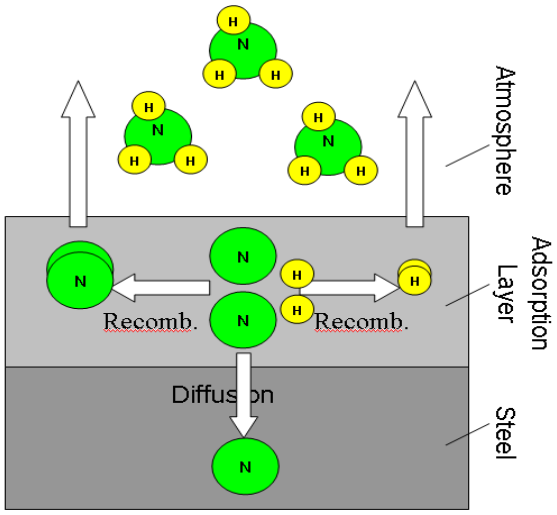

Figure 2.4 : Diffusion mechanism of gas nitriding [7]

The most important phases occurring during nitriding in the compound layer are the γ′ and ε phases. These two phases, γ′ and ε, can be conceived as typical interstitial compounds with the iron atoms arranged in a cubic close-packed fashion in the γ′ phase and in a hexagonal close-packed fashion in the ε phase (Fig. 2.5 a-b). In both phases the octahedral interstitial sites are partially occupied by nitrogen with long-range order, leading to space group Pm3m for γ′ and $P6_322$ for ε. Figure 2.6 presents reaction rates of ammonia decomposition (straight line) and nitride formation(dashed line), as well as calculated values for temperature 450°C. Initially, (region A)

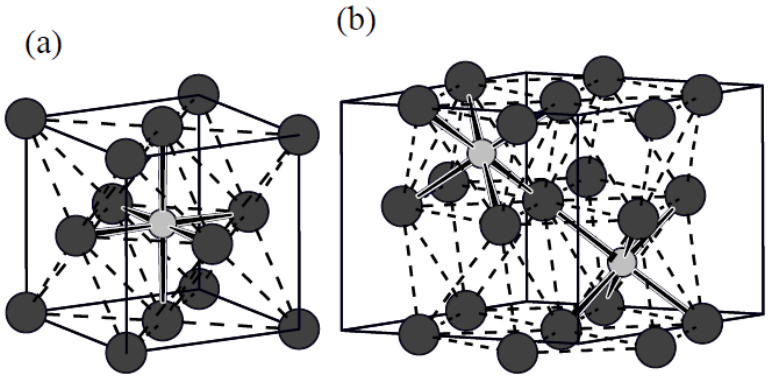

Figure 2.5 : Crystal structure of (a) γ´-Fe_4N_{1-y} and (b) ε-Fe_3N_{1+x}. The darker spheres represent the iron atoms and the lighter spheres the nitrogen atoms. Fe-Fe 'bonds' are indicated by dashed lines and Fe-N 'bonds' are indicated by solid bold lines [5]

decomposition is started, nitrides are not formed. Nitrides are not formed until critical value. The rate of the decomposition reaction reached its maximum value when the nitriding reaction just started. Nitriding reaction (region B) started after a minimal nitriding potential needed for nitriding reaction to be commenced, equal to ca. 0.001 Pa-1/2, was reached. After maximum decompotison reaction rate is obtained under given conditions (450°C) the nitriding process took place on two phases α-Fe(N) and γ′-Fe_4N (region B). Before the phase transformation of α-Fe(N) to γ′-Fe_4N was almost completed, the nitriding reaction slowed down and its rate reached its minimum value. Along with increase of content of γ′-Fe_4N phase, the rate of ammonia decomposition drops to zero. This means that

the ammonia decomposition on γ′ phase is slower than that on the α phase. An increase in the rates of both reactions was observed after a complete phase transformation (region C) [7].

2.1.2 Thermodynamics of nitriding

A part of the standard Fe–N phase diagram is shown in Figure 2.7. The ferrite (α-Fe) and austenite (γ-Fe) phase fields, and the γ´-Fe_4N_{1-x} and ε-Fe_3N_{1+y}phase fields are indicated [9]. The relation between process parameters and morphology of the produced surface layer is of great interest for the realisation of well defined

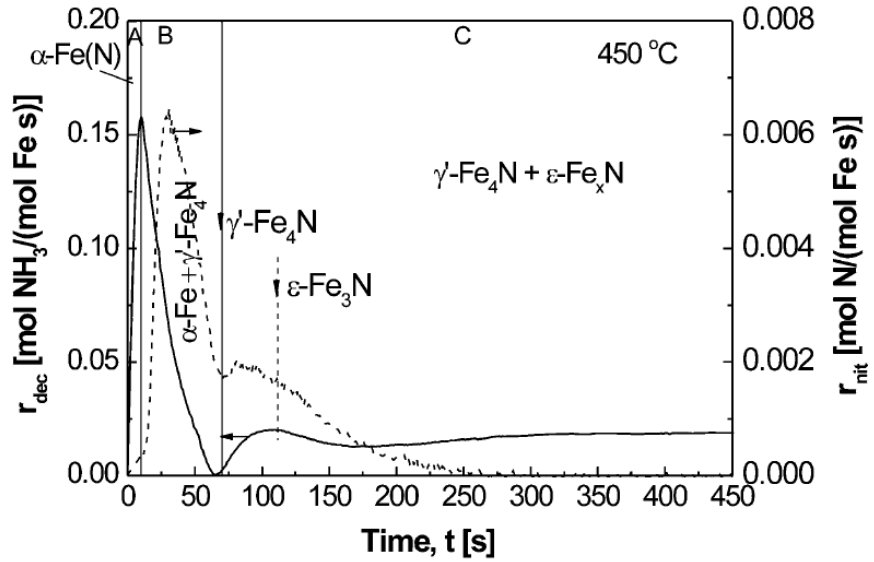

Figure 2.6 : Reaction rates at 450°C - nitriding reaction, rnit, and catalytic ammonia decomposition reaction [8]

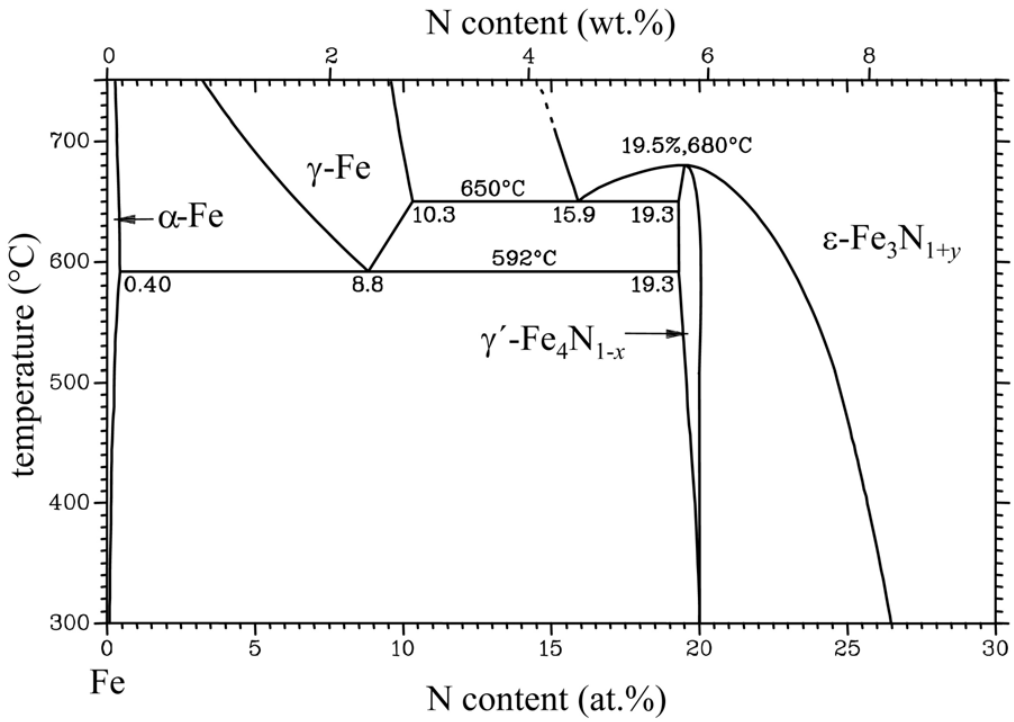

Figure 2.7 : Fe–N phase diagram [9]

compositions and structures and, hence, properties. For this reason it is necessary to have a reproducible, controllable processing. Well controlled nitriding requires knowledge and control of the chemical potential and the corresponding nitrogen

activity as provided by an ammonia/hydrogen gas mixture. N_2 gas as nitrogen donating medium is not suitable for gaseous nitriding because the nitrogen activity at atmospheric pressure is to low.

Gaseous nitriding involves a metal-gas reaction between solid ferrite and an ammonia/hydrogen gas mixture. Thereby nitrogen becomes dissolved in the solid ferrite matrix according to the following reaction [9];

$$NH_3 \Leftrightarrow \underline{N}_{\alpha-Fe} + \frac{3}{2}H_2 \qquad \textbf{(2.10)}$$

where $\underline{N}_{\alpha-Fe}$ represents the in the ferrite matrix dissolved nitrogen.

The chemical potential (i.e. Gibbs free energy μ) of nitrogen, dissolved in the solid ferrite matrix is defined as

$$\mu_{\underline{N}_{\alpha-Fe},s} = \mu^o_{\underline{N}_{\alpha-Fe},s} + RT\ln a_{\underline{N}_{\alpha-Fe}} \qquad \textbf{(2.11)}$$

Where $\mu^o_{\underline{N}_{\alpha-Fe},s}$ denotes the chemical potential of nitrogen in the solid (s) reference state (i.e. ferrite), $a_{\underline{N}_{\alpha-Fe}}$ represents the activity of nitrogen in the dissolved state with respect to the reference state (in the reference state $a_{\underline{N}_{\alpha-Fe}} = 1$), R is the gas constant and T the absolute temperature. $\mu^o_{\underline{N}_{\alpha-Fe},s}$ is temperature dependent at the selected pressure of the reference state. There is no precondition for the selection of the reference state. Hence, the relevant reference state must be specified for the discussion of activities.

In a gas mixture the chemical potential of a gaseous constituent i is defined by

$$\mu_{i,g} = \mu^o_{i,g} + RT\ln\left(\frac{f_i}{f_i^o}\right) \qquad \textbf{(2.12)}$$

where $\mu^o_{i,s}$ is the chemical potential of i in the gaseous (g) reference state (temperature dependent at the selected pressure of the reference state), fi denotes the fugacity of i in the gas mixture and f_i^o represents the fugacity of i in the reference

state. Assuming an ideal behaviour of the considered gases or constant fugacity coefficients equation 2.13 can be written as

$$\mu_{i,g} = \mu_{i,g}^{o} + RT\ln(\frac{p_i}{p_i^o}) \qquad \textbf{(2.13)}$$

where pi is the partial pressure of i and p_i^o represents the pressure of i in the reference state.

Thermodynamic equilibrium between solid ferrite and the ammonia/hydrogen gas mixture requires that the chemical potentials of nitrogen in the gas phase and in the solid phase (i.e. specimen surface) are equal. If this prevails, it follows on the basis of equations 2.14 to 2.16

$$\mu_{NH_3,s} = \mu^{o}_{N\,\overline{\alpha-Fe},s} + \frac{3}{2}\mu_{H_2,g} \qquad \textbf{(2.14)}$$

and from equation (1.5) it follows

$$\mu_{N\,\overline{\alpha-Fe},s} = \mu^{o}_{NH_3,g} - \frac{3}{2}\mu^{o}_{H_2,g} + RT\ln(\frac{p_{NH_3}}{p_{H_2}^{3/2}}) \qquad \textbf{(2.15)}$$

where it should be emphasised that the pressure of the reference state is selected as one atmosphere (p_i^o = 1 atm) and p_i must have the same unit as p_i^o (i.e. atmospheres). Hence, the activity of nitrogen dissolved in the solid at a constant temperature is controlled by the ratio

$$K_N = (\frac{p_{NH_3}}{p_{H_2}^{3/2}}) \qquad \textbf{(2.16)}$$

which is called nitriding potential. The nitriding potential (i.e. nitrogen activity at the specimen surface) can be adjusted by the composition of the gas mixture in the flow-through furnace. The composition of the gas mixture (i.e. mole fractions of ammonia and hydrogen) can be controlled to a high degree of accuracy with well calibrated mass-flow controllers (variance within 1 % of the adjusted value in ml/min). Besides temperature and time the nitriding potential is the most decisive, independent

parameter for a controlled nitriding processing [8]. The nitriding potential K_N governs the chemical potential of nitrogen in the gas phase and, hence, the activity of nitrogen dissolved in Fe at the interface between Fe and the ammonia/hydrogen gas mixture. According to Figure 2.7, which shows the phase fields for the Fe–N system classically as temperature over nitrogen concentration, Lehrer determined the borders of the Fe–N phase fields with respect to the temperature and the nitriding potential and drew the so called Lehrer diagram [9]. Such a Lehrer diagram is depicted in Figure 2.8. Besides the phase boundaries, the Lehrer diagram in Fig. 2.8 shows additionally lines of constant nitrogen concentration (i.e. isoconcentration lines) [9]. An in this way extended Lehrer diagram provides not only the adjustment of a certain phase but also of a certain nitrogen concentration at the Fe specimen surface.

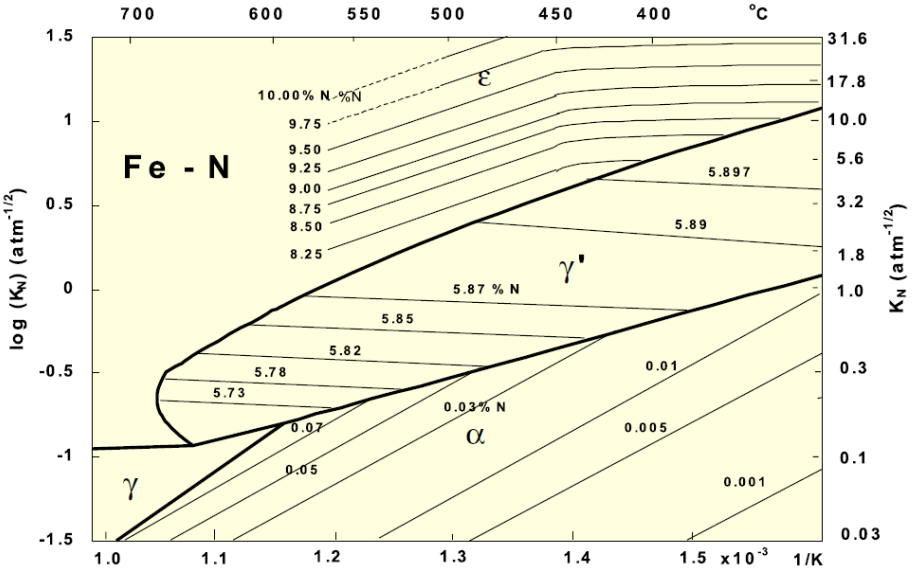

Figure 2.8 : Lehrer diagram with isoconcentration lines, redrawn according to [10] indicating the equilibrium Fe–N phase fields with respect to the temperature and the nitriding potential at the Fe/gas atmosphere interface [11]

2.2 Morphology and Constitution of the Nitrided Layer

2.2.1 Morphology of the nitrided layer

It is assumed that the growth of the nitrided zone during nitriding is controlled by the diffusion of nitrogen atoms over the octahedral interstices of the iron sublattice. A local equilibrium between dissolved nitrogen in the ferrite matrix and the ammonia/hydrogen gas mixture is only achieved at the specimen surface. Beneath

the surface the nitrogen concentration decreases, due to inward diffusion, and hence the chemical potential of nitrogen in ferrite decreases with increasing depth.

One parameter is nitriding potential which effects to grow up compound layer. If the nitiding potential does not allow the development of iron nitrides, the nitrided zone consists only of ferrite with a concentration depth gradient of dissolved nitrogen (α-Fe region in Figure 2.9 and maximum nitrogen solubility in ferrite in Fig. 2.7). If the nitriding potential allows iron nitride formation, it depends on the local equilibrium concentration of nitrogen at the surface (Fig. 2.7 and 2.8) whether γ-iron nitride develops or a layer of ε iron nitride together with γ′ iron nitride beneath [5].

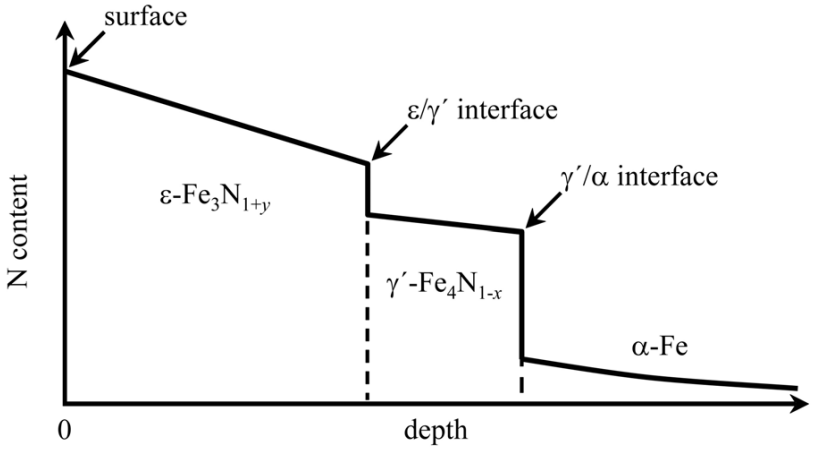

Figure 2.9 : Schematic nitrogen concentration depth profile of the nitrided zone of a pure α-Fe matrix [5]

Another parameter is temperature which effects to occur compound layer especialy in two stage gas nitriding process. The principle of the procedure is to reduce the amount of avaliable nitrogen for surface diffusion and to ensure a rapid diffusion by raising the process temperature. The temperature for the second stage must be carefully selected. Selection of higher process temperatures poses the risk of grain-boundry networking with iron nitrides at the periphery of grain boundries, leading to premature component failure at sharp corners (Fig 2.10 and 2.11). When considering use of the two-stage process, it may be prudent not to employ the higher temperature. The higher temperature does not influence the final hardness value, only the diffusion rate [4].

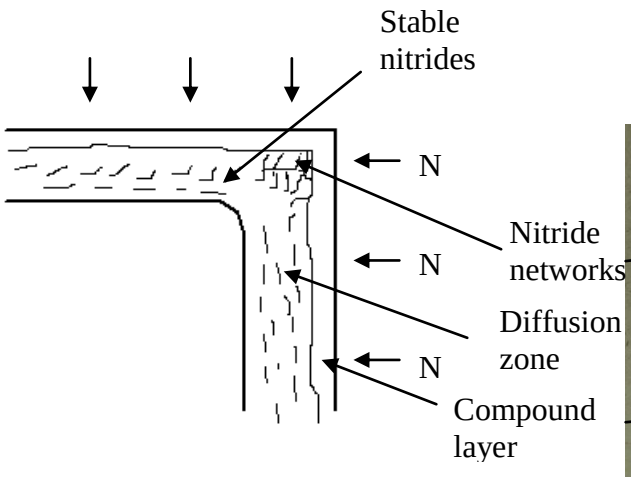

Figure 2.10 : Illustrating the effects of nitrogen enrichment (nitride networking) at the corner [4]

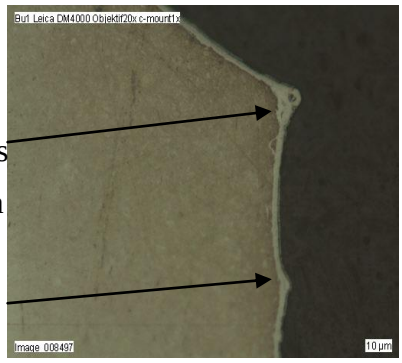

Figure 2.11 : Microscope image of nitrided Steel (500°C-10h, K_N:0,40)

2.2.2 Constitution of the nitrided layer

The formation of nitrides upon nitriding changes the microstructure of the ferrite matrix in the nitrided zone of the specimen, made of pure iron, an iron-based alloy or steel. With respect to the present nitrides and the layer constitution the nitrided zone can be subdivided into the compound layer and the diffusion zone (Fig. 2.12).

The compound layer is a closed layer at the specimen surface consisting of the hcp ε iron nitride together with fcc iron nitride beneath or only γ′ iron nitride without ε iron nitride above (Section 2.1.1). The demanded tribological and anti-corrosion properties of nitrided specimens are benefited by the compound layer.

The part of the nitrided zone beneath the compound layer, in which nitrogen largely is dissolved interstitially in the ferrite matrix, is called “diffusion zone”. In the diffusion zone of pure α-Fe, precipitates of γ'-Fe_4N_{1-x} and α''-$Fe_{16}N_2$can be present. In case of iron-based alloys or steels, containing nitride forming elements such as Ti, V, Mo, Cr or Al, so called “inner nitrides” can precipitate, which are to a large extent responsible for an improvement of the fatigue behaviour [9].

2.3Mechanical and Technological Properties of the Nitrided Layer

The nitriding process is more favourable process because of its applications which both fatigue strentgh by hardness and residual stress and corrosion resistance can be

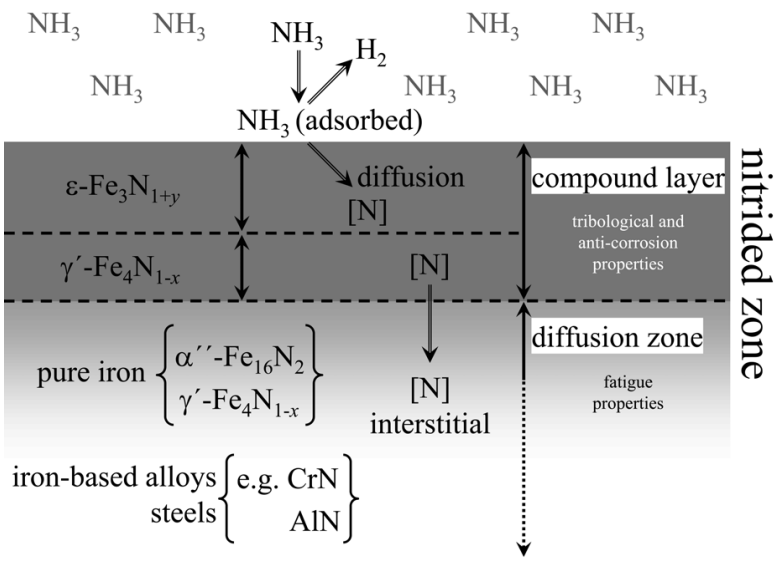

Figure 2.12 : Schematic illustration of the nitriding process at the specimen surface (pure iron or iron-based alloy) [9]

both fatigue strentgh by hardness and residual stress and corrosion resistance can be achieved at the same time. According the nitriding potential which is responsible surface nitrogen content, nitride precipitation and inward diffusion can be changed which occurs because of excess nitrogen and also residual stress behaviour can be changedby different precipitation. There are explained below effect of excess nitrogen and residual stress on fatigue stress in nitrided material.

corrosion resistance is achieved by gas nitriding process with post treatment which is mentioned in Section 2.3.3.

2.3.1 Residual stresses

Presence of excess nitrogen in the nitrided layer changes the residual stress behaviour because of the misfit precipitation. Residual stresses are self-equilibrating stress existing in materials under uniform temperature conditions without external loading. They often arise in materials in consequence of processing steps such as heat treatment or machining. Residual stresses can have many different origins (e.g. mechanical, thermal, plastic or due to phase transformation such as inner nitride precipitation) but they are all the result of misfit.

These misfits can occur between different parts, different phases, or different regions within the same part. Depending on the scale over which they self-equilibrate residual stresses can be subdivided into macrostresses and microstresses.

Macrostresses are defined as a Type I which occurs overlarge distances. Microstresses are defined as a Type II and Type III, which vary over the grain scale and the atomic scale (Type II). The misfitting regions in case of microstresses are of microscopic and submicroscopic dimensions. Significant Type II stresses occur when the microstructure consists of several phases or due to phase transformations. Type III stresses originate from the coherency misfit strain at interfaces and from dislocation stres fields.

Residual stresses play a decisive part when considering various damage processes, such as crack initiation and propagation, brittle fracture, high- and low-cycle fatigue, contact fatigue. It must be noted that besides the residual stress distribution, the kinetics of most damage processes is also influenced by several other important factors, including type of external loading, microstructure morphology, properties of nitrided depth, part geometry, and surface conditions. It is generally assumed that the compressive residual stresses offset the adverse effects of factors such as quench embrittlement and intergranular fracture to which high-nitrogen microstructures are susceptible, and they increase the fracture and fatigue resistance of direct-quenched parts to levels that provide good engineering performance [3].

To understand the development of residual macrostresses in the diffusion zone of the nitrided layer, an extremely simplified description is given in the following: the initial state is an unnitrided specimen (Fig. 2.13-a). During nitriding nitrogen becomes incorporated into thesurface of the specimen where it forms inner nitride precipitates with the present nitride-forming elements (e.g. Cr, Al, etc.) in the diffusion zone. In Fig. 2.13-b the nitrided zone and the unnitrided core of the specimen are considered notionally separately. The difference in specific volume between the matrix and the developed nitrides expands the nitrided layer. In fact, (Fig. 2.13-c) the nitrided layer and the unnitrided specimen core are attached to each other and a self-equilibrating stress state has to be reached. As a result of this equilibrium stress state, a residual macrostress state of compressive character is induced in the nitrided zone, whereas a residual macrostress state of tensile character responds in the unnitrided core [9].

In the Figure 2.13 shows (a) As initial state an unnitrided specimen is considered in which nitrogen becomes incorporated upon nitriding. (b) The formation of inner nitrides in the diffusion zone brings about a theoretical expansion of the nitrided zone

(see text). (c) The resulting equilibrium stress state induces a residual stress state of compressive character in the nitrided zone and consequently a residual stres state of tensile character in the unnitrided core beneath [9].

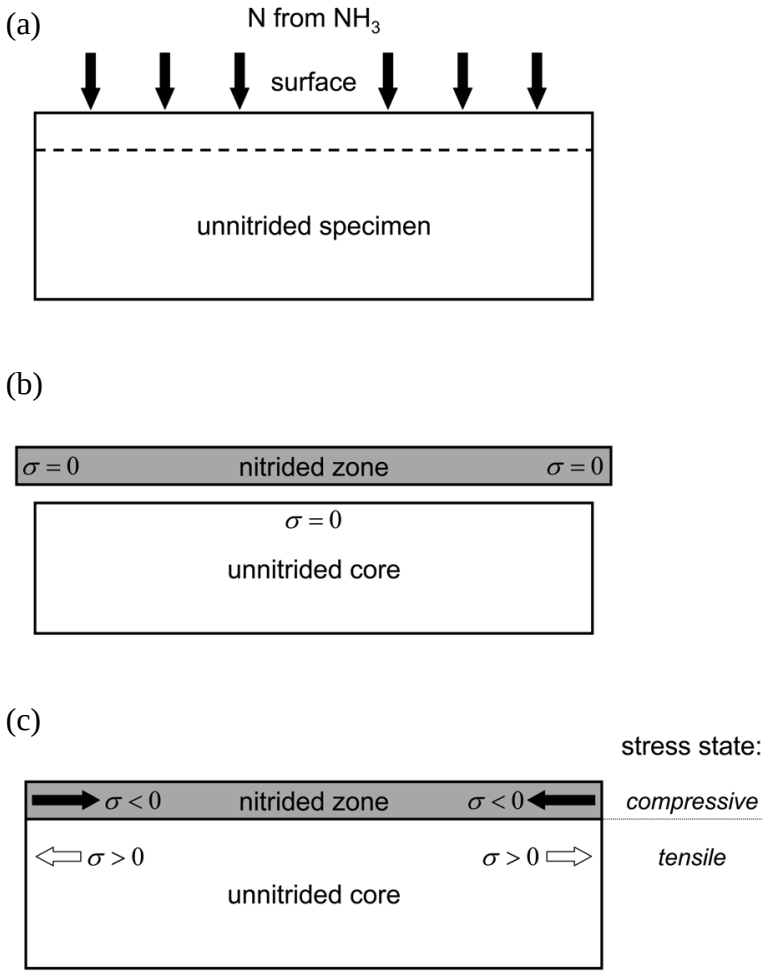

Figure 2.13 : Schematic illustration of the residual macrostress development in a specimen during nitriding [9]

2.3.2 Fatigue strength

During gas-nitriding two layers can be formed which is mentioned before: the compound layer, consisting of iron nitrides, on top of the diffusion layer, consisting of an iron matrix containing precipitates of alloying element nitrides. This diffusion layer is responsible for the improvement in fatigue strength, as the hard compound layer is very brittle and has little mechanical strength. Generally, the fatigue limit increases with increasing diffusion layer thickness, but the relation is non-linear and depends on the local stress concentration. Gas nitriding with different process parameters such as temperature, time effect on diffusion layer thickness which

supply fatigue strength and nitriding potential effect on compound layer thickness which causes crack initiation because of brittle properity. Therefore, there should be optimized nitriding potential to control compound layer thickness, temperature and time to control diffusion layer thickness. If the nitriding potential is sufficiently high, the thickness of the diffusion layer depends for a given steel on nitriding temperature and time only. In industrial practice nitriding is invariably performed at the highest temperature possible (580°C) in order to minimize the process cycle time. However, as nitriding is essentially a precipitation process, nitriding at a high temperature does not automatically lead to the precipitate size and density required for the highest fatigue resistance. Nitriding at lower temperatures could lead to finer precipitates and a better fatigue resistance [12].

Surface hardening and compressive residual stresses usually increase the fatigue limit of steels. Nitriding is beneficial in high cycle fatigue and can result in a transition fromsurface failure to internal failure. On the other hand, it might be disadvantageous in low cycle fatigue where cracks can initiate rapidly at the surface which has lower ductility than the core.

In surface-hardened steels, cracks can initiate and propagate at the surface. However, if the enhanced hardness hinders initiation and the residual compressive stresses slow down propagation, the initiation site of the crack leading to failure can be shifted fromthe surface into the core of the specimen at internal defects; non-metallic inclusions reportedly being the most frequent ones. The Stress (S)–Number of cycle (N) curve of a high-strength steel can be described as a "stepwise curve" (Fig. 2.14) that results fromthe superposition of two curves, one being associated with surface failure, and the other with internal failure. There is sometimes a marked transition between the two curves, which corresponds to the surface fatigue limit. Though the internal failure mode is normally observed at very high fatigue lives (10^7–10^9 cycles), surface strengthening can shift the transition between surface and internal failure modes (point A) at lives as short as 10^4–10^5 cycles (point B). Unlike surface cracks, internal cracks are not affected by surface defects and environment factors (e.g. corrosion, hydrogen embrittlement or simply air oxidation). Actually, internal cracks initiation and growth depends on the core properties only, e.g. hardness and

flaw size [13]. For nitrided specimens the initiation of fatigue cracks, as a rule, occurs at the interface (nitrided layer – basic metal) at nonmetallic inclusions, and

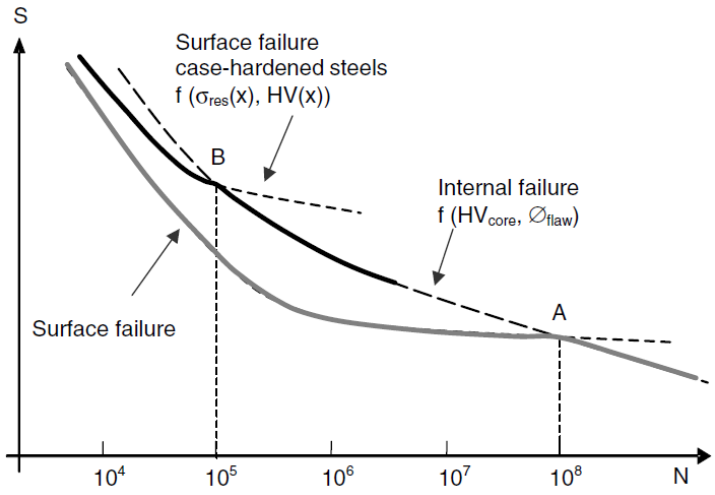

Figure 2.14 :‘Stepwise’ Stress (S)–Number of cycle (N) curves (thick lines) [13]

that results in formation of the surface of fatigue fracture. Thus, we see that increase of gas nitriding time, results in the increase of hardness of a nitrided layer, however plasticity of the basic metal sharply decreases what may result in sudden brittle failure. Therefore not always it is necessary to seek for maximum hardness on a surface of structural steels after nitriding. Also it is necessary to take into account operating conditions of nitrided parts because the conditions of damaging are various, for example fatigue or wear [14].

2.3.3 Effect of pre oxidation on nitrided layer

Certain impurities can form a passivating layer on steel surfaces during nitriding. These impurities either delay the formation of the compound layer and the development of a diffusion zone or simply stop their formation altogether. Besides, there are indications that deformation of workpiece surfaces plays a role in the occurrence of inhomogeneous nitriding as well. The presence of very thin layers of impurities on workpieces may be due to the metalworking and cleaning operations that are carried out before nitriding. Metalworking operations often require fluids to cool or lubricate, and these fluids are usually removed by cleaning steps before nitriding. When thin layers of impurities on the steel surface are indeed responsible

for inhomogeneous nitriding, these impurities should either originate from the metalworking fluids due to poor cleaning or from the cleaning agents themselves [15]. Figure 2.15 shows cross sections of nitrided specimens. Figure 2.15-a is the microstructure of the nitrided specimen without pretreatment. The gray part on the upper side is the resin for embedding the specimen, whereas the white part is the austenite matrix. No nitrided region is observed in Figure 2.15-a. Small amound of nitrided region is formed very locally in Figure 2.15-a. After pre-oxidation at 300°C. The specimen nitrided after pre treatment at 400°C has a nitrided layer with a near uniform thckness (Fig. 2.15-c). The specimen nitrided after pre treatment at 1000°C exhibits homogeneous nitriding (Fig. 2.15-d) but a layer with different quality is formed on the nitridied layer. It maybe Fe_3O_4 layer detected by XRD (Fig. 2.16-c) [16].

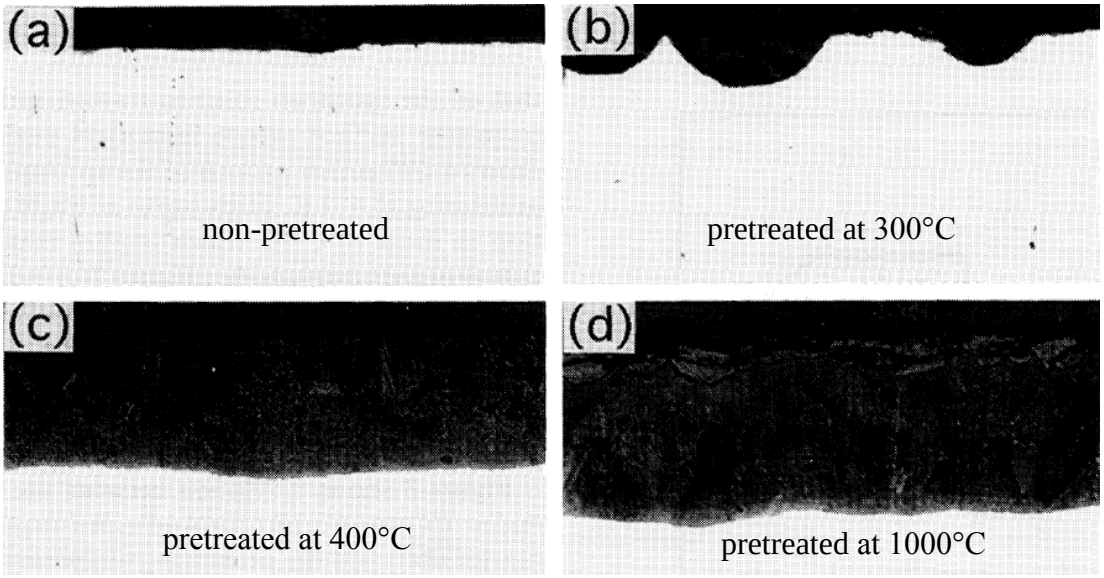

Figure 2.15 : Optical microstructure of longitudinal sections of nitrided specimens [16]

2.3.4 Effect of post oxidation on corrosion resistance

The compound layer thickness can change as function of nitriding potantial, temperature and time. Therefore, corrosion resistance of material depends on compound layer thickness and also these process parameters. Effect of nitriding duration and nitriding potantial on compound layer thickness can be seen from Figure 2.17. Compound layer thickness increaes by increasing the nitriding potantial and also nitriding time. This means that, corrosion resistance increases by these parameters (K_N and time). Nitiriding temperature may also play a critical role on the

compound layer growth. Temperature effect on corrosion resistance is shown in Figure 2.18 that are achieved by electrochemical corrosion tests.

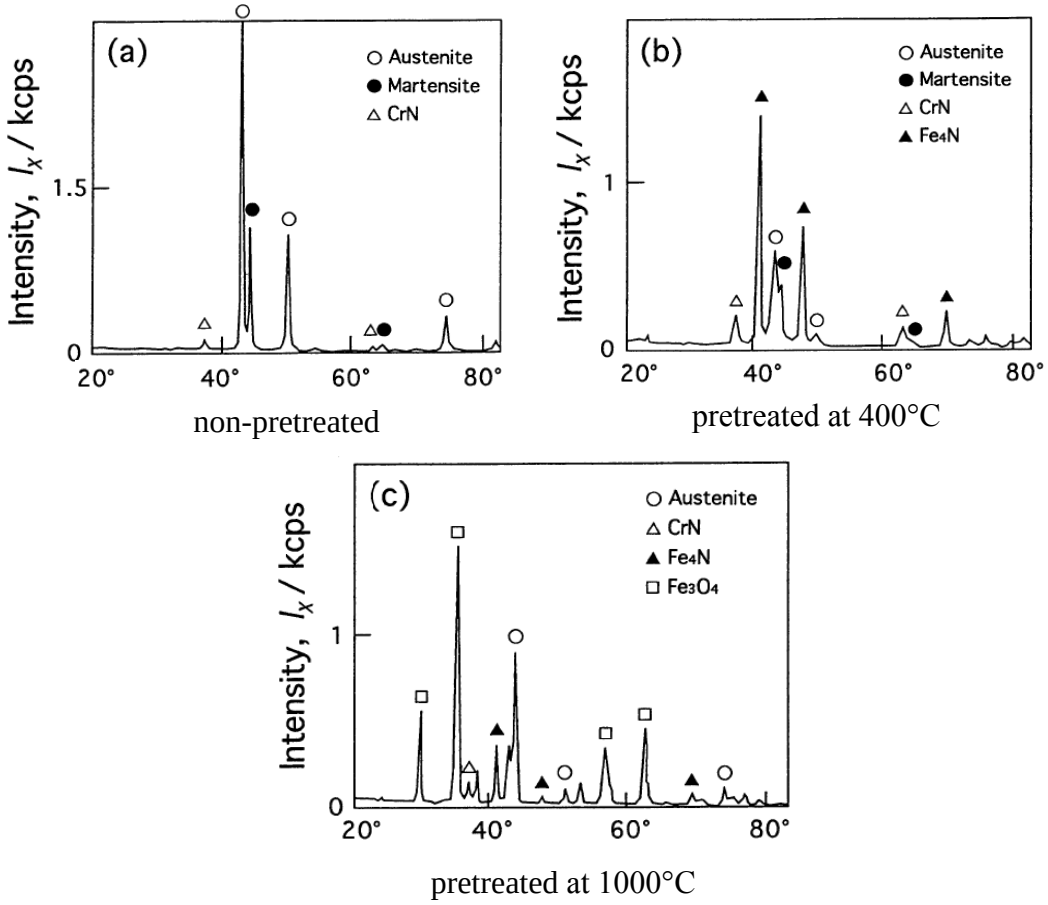

Figure 2.16 : X-Ray diffraction patterns on the surface of nitrided specimens [16]

The corrosion protective properties of the compound layer relies more on porosity than thickness. The compound layer is usually porous [19] and this tends to decrease the corrosion resistance. A possible solution to improve corrosion resistance consists in the post-oxidation treatment. This second treatment causes the subsequent partial decomposition of the Fe-carbonitrides in oxides (mainly Fe_3O_4) which lead to a decrease in the micro porosity [20]. Iron-oxide phase diagram is shown Figure 2.19. In the oxidizing process, free iron and iron nitrides must be converted to a stable iron oxide (Fe_3O_4) such that a chemically resistant protective layer of approximately 1–2 μm thick is added to the compound layer (Fig. 2.20). The important factor at the post oxidation process is that the oxidation has to be controlled to avoid hematite (Fe_2O_3) formation and produce pure magnetite (Fe_3O_4) which is highly corrosion resistant [22].

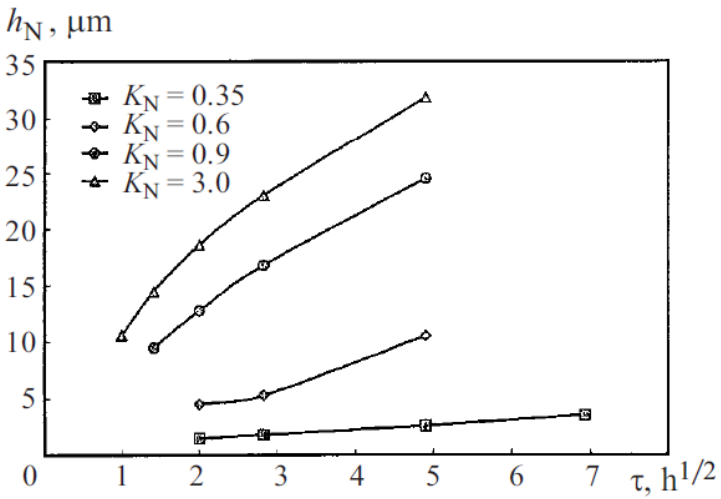

Figure 2.17 : Effect of the duration of nitriding at 570°C and of nitrogen potential K_N on the thickness of the layer of chemical compounds (h_N) in steel 42CrMo4V [17]

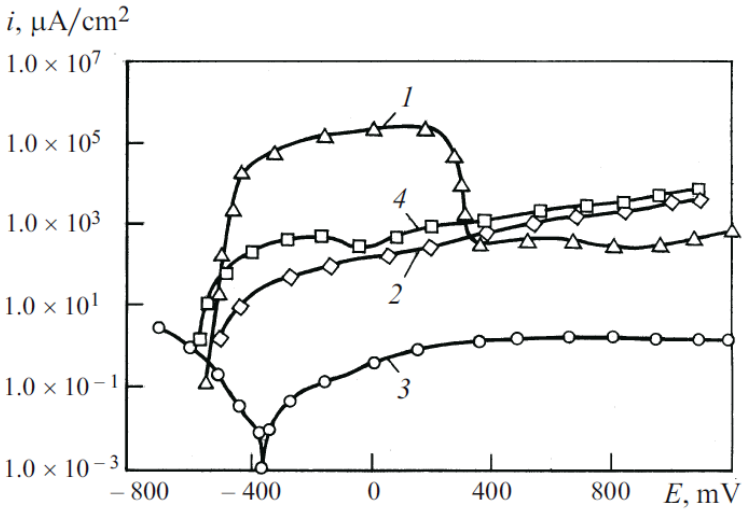

Figure 2.18 : Curves describing anode polarization of steel 1010 in 20% solution of H_3PO_4: 1) before nitriding; 2, 3, 4) after nitriding by modes 2 (490°C), 3 (560°C), and 4 (580°C) [18]

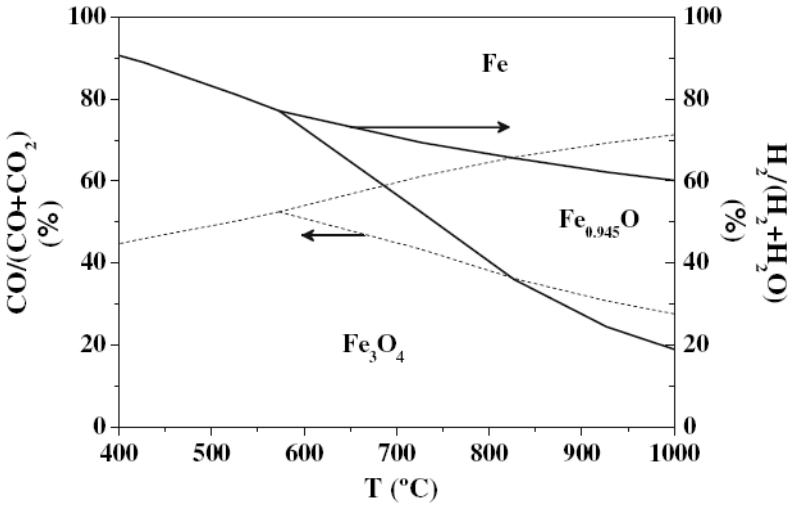

Figure 2.19 : Bauer–Glaessner diagram: equilibrium compositions of the gases involved in the redox reactions of H_2/H_2O and CO/CO_2 with F_3O_4 (magnetite), $Fe_{0.945}O$ (wustite) and Fe [21]

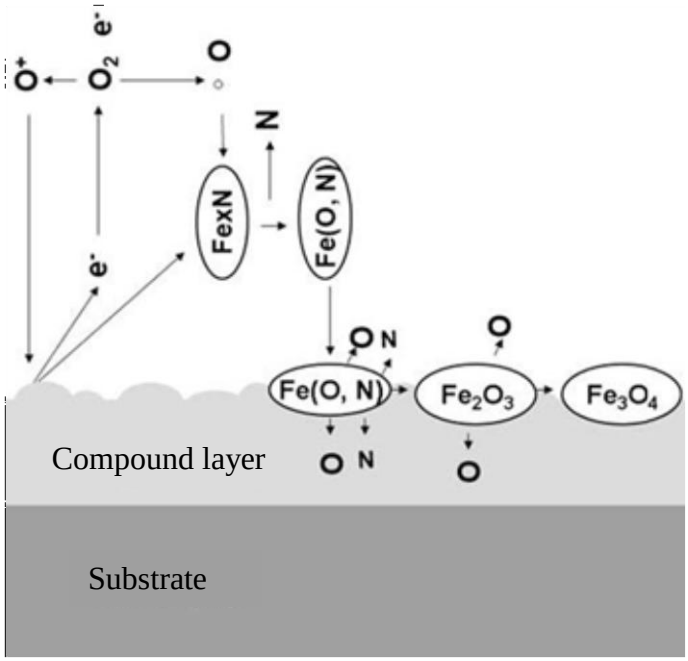

Figure 2.20 : Schematic illustration of proposed mechanism for oxide layer formation in post-oxidation process [22]

3. EXPERIMENTAL PROCEDURE

In this section the experimental details of the study conducted on the controlled gas nitriding of diesel injector parts will be given.

3.1 Specimens and Specimen Preparation

This thesis was done to achieve high fatigue strength and corrosion resistance for Common Rail (CR) diesel injector bodies in Robert Bosch Turkey (RBTR).

Three different samples were used in the experimental studies for trials (Fig.3.1).

First serial trials were done by high pressure connectors (Fig 3.1-a) because of their simple geometry in which there are no intersections of the hole in high pressure connectors.

After optimization of the nitriding parameters with high pressure connectors, this information was transferred to more complex Common Rail (CR)-Injectors (Fig 3.1 b).

Experiments related to corrosion resistance were conducted on through hole specimens (Fig 3.1-c)

High Pressure Connectors and CR-Injectors were prepared by Cengiz Makina, İstanbul, and in Bamberg/Germany respectively. Through hole specimens were machined in RBTR.

Tempered steels (hardening at 1040°C-2,5 h, quenching with N_2 at 6 and 2,5 bar and then tempering at 510°C- 2 h and 610°-2 h) were used for the preparation samples. Hardness of samples are seen in Table 3.1 below.

Prio to nitriding experiments oiled sample surface were cleaned in a commercial alkaline cleaner (Neutrapan 5088- Henkel)

Table 3.1: Material composition of components in experimental investigations

Geometry	Material composition	Core hardness (HV)
High Pressure connector	42CrMo4	350
CR-Injector	50CrMo4	350
Through Hole Specimen	50CrMo4	350

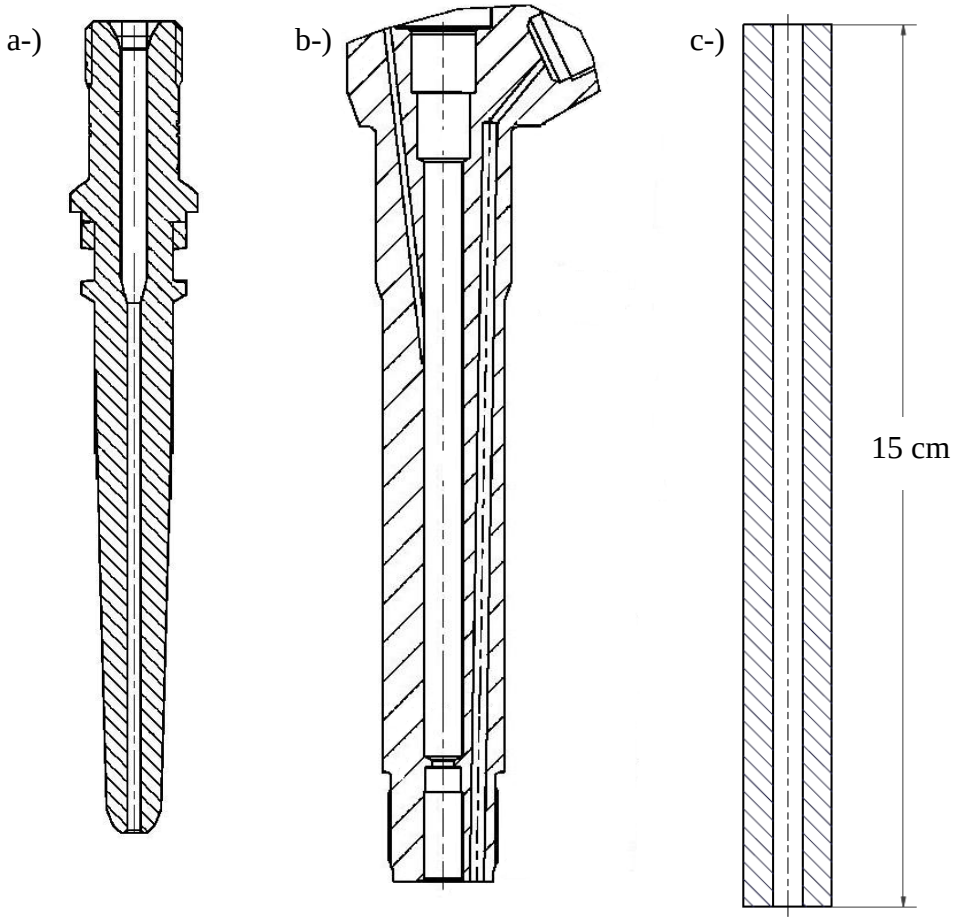

Figure 3.1 : Experimental specimen geometries a) High pressure connector, b) CR-injector, c) Through hole specimen

3.2 Gas Nitriding

The nitriding experiments were conducted in an industial gas nitriding furnace (IPSEN, VDR-type) (Fig. 3.2)

Figure 3.2: Industrial nitriding furnace in RBTR

The samples were loaded only from the top of the furnace within the basket (Fig. 3.3-b)

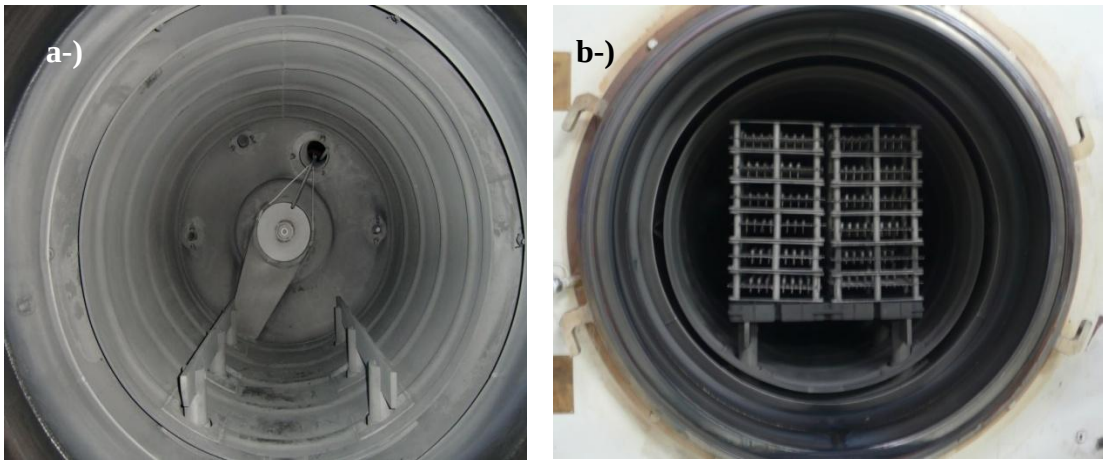

Figure 3.3 : Images of industrial furnace a) retort, b) retort with load basket

Gas nitriding process has three main steps: 1. Heating 2. gas nitriding and 3. cooling. An example of of gas nitriding process flow is given in Figure 3.4. For making the process contollable precisely, the partial pressure of nitrogen was measured by sensors located in suitable places in the furnace. A feed back mechnasim was also

present for keeping the nitrogen partial pressure same throughout the whole experiment duration.

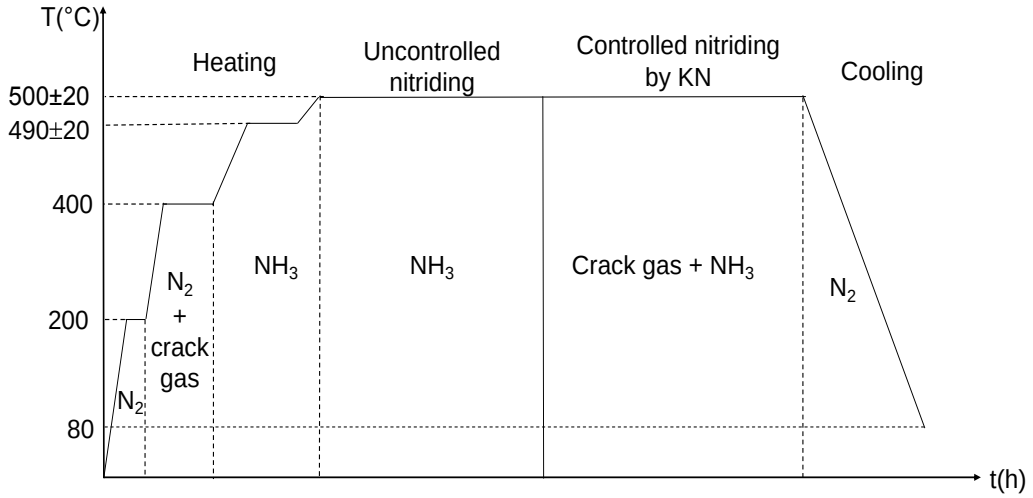

Figure 3.4 : General flow of gas nitriding process

3.2.1 First trial series with high pressure connector

There were three main process parameters for the gas nitriding process which should be optimized. These were nitriding potatial (K_N), temperature and time. For the first trial series an experimental matrix which is shown Table 3.2 was prepared. For getting a minimum compound layer thickness to prevent crack initiation literature a nitriding potential (K_N) of 0.40 has been selected [11,17,18] This K_N value represents thin compound layer region according to the Lehrer diagram (Fig. 2.8). To start the reaction on the surface, there needed to be enough nitrogen concentration so trails has been started by one hour uncontrolled nitriding which means it has high nitriding potantial. The aim of first trails was to increase fatigue resistance. For this reason, it was decided to use four different nitriding durations given in Table 3.2. Other important parameter is temperature. A modearate nitriding temperatures of 500°C and 520°C were selected since it is well known that high temperature decreases compressive residual stress which is not benficial for fatique resistance [11,14].

Table 3.2: Experimental matrix for the first trial series with high pressure connector

Trial Nr.	Nitriding potential (K_N)	Temperature (°C)	Time (h) uncontrolled + contolled nitiriding durations
1	0,40	500	1+9
2	0,40	500	1+39
3	0,40	520	1+5
4	0,40	520	1+23

3.2.2 Second trial series with CR-injector

New experiments were designed for this injectors, relying on the results of the first series of experiments (Table 3.3).

Table 3.3: Experimental matrix for the second trial series with CR-injector

Trial Nr.	Nitriding potential (K_N)	Temperature (°C)	Time (h) uncontrolled + contolled nitiriding durations
5	0,40	520	1+5

3.2.3 Third trial series with through hole specimen

These specimens were used to investigate homogenitiy and corrosion resistance by pre and post-oxidation treatments. Therefore, an experimental matrix with four different pre-oxidation treatments by air and three different nitriding parameters were prepared (Table 3.4)

Table 3.4: Experimental matrix with through hole specimen

Gas Nitriding (K_N=0.40)					
Pre-oxidation	520°C (1+5) h*	520°C (1+4+1) h**	520°C-(1+4+1) h** cooling NH3	480°C (5+5) h***	**Post-oxidation**
350°C-1h	1	16	31		450°C-1h
450°C-1h	2	17	32		
450°C-4h	3	18	33		
550°C-1h	4	19	34		
350°C-1h	5	20	35		
450°C-1h	6	21	36		450°C-4h
450°C-4h	7	22	37		
550°C-1h	8	23	38		
350°C-1h	9	24	39		
450°C-1h	10	25	40		550°C-1h
450°C-4h	11	26	41		
550°C-1h	12	27	42		
w/o+	13	28	43	46	450°C-1h
w/o	14	29	44	47	450°C-4h
w/o	15	30	45	48	550°C-1h

+w/o: without

*First 1 h uncontrolled, rest of time controlled nitriding with K_N

**First and last 1 h uncontrolled, rest of time controlled nitriding with K_N and then cooling in NH_3

***First 5 h uncontrolled, rest of time controlled nitriding with K_N

3.3 Specimen Characterization

After preparation of the nitride samples, structure and thickness of the layer were investigated with optical microscope after sutiable metallographic preparation. Scanning Electron Microscope (SEM) was also used in cross sectional investiagtions. Glow discharge optical emisison spectroscopy with depth profiling (GDOES) was used for the determination of the chemistry of the nitride layer. Hardness of the layers were measured from their metallographically prepared cross sections with micro hardness tester. Residual stresses were measured with X-ray diffraction technique (XRD) and pulsation tests were usedfor the evaluation of fatigue resistance. Corrosion resistance of the samples were determined by salt spray testing.

3.3.1 Optical microscope (OM)

For optical microscopy investigations, pieces were cut from the samples and prepared after embedding (Struers CitoPress-20). Aftermetallographical preparation samples were polished with 1 μm diamond paste. For etching Klemms-I (2 g Potassium metabisulfite ($K_2S_2O_5$), 40 g Sodium thyosulfate ($Na_2S_2O_3$), 100 ml H2O at 0°C for about 2 min)Adler (60 g Ferric chloride hexahydrate ($FeCl_3x6H_2O$), 12 g Copper ammonia chloride $(NH_4)_2[CuCl_4]x2H_2O$, 100 ml ml water (H_2O), 200 ml HCl at 25°C for 5 s) solutions were used. These cross sections were investigated with optical microscopy usinga Leica DM4000M microscope. The micrographs were recorded with a digital camera (Leica DFC280).

3.3.2 Hardness measurement

Hardness-depth profiles were obtained by carrying out hardness measurements across the cross-sections of the nitrided specimens using a Shimadzu HMV-2 hardness tester, with an applied load of 500 g.

3.3.3. Scanning electron microscope (SEM)

For scanning electron microscopy (SEM) the same (etched) cross-sections were used as for optical microscope. The SEM micrographs were taken with a Zeiss EVO50 operating at 20 kV.

3.3.4 Glow discharge optical emission spectroscopy (GDOES)

The concentration profiles of nitrogen, carbon and oxygen in the nitride layers have been determined by GDOES (GDA 750 (Spectruma Analytic GmbH), which has the ability of analyzing of surface layers, up to a depth of about 100 μm. The semiquantitative analysis of carbon and nitrogen in compound and diffusion layers was determined.

3.3.5 Salt spray (fog) test

The salt-spray (fog) test was done for 5.5 h in accordance with ASTM B117 [24] and DIN EN ISO 9227:2006-10 [25] standards by using a salt spray cabinet (Erichsen, Model 606/400M). The results were evaluated according to DIN EN ISO 4628-3:2003 standard [26].

3.3.6 Stress analysis with X-Ray diffraction (XRD)

XRD stress analysis was done by Seifert Micro Beam XRD 3003 PTS XRD diffractometer equipped with a Cr-Tube as X-Ray source. In the system a linear detector (Meteor1D Semiconductor Strip Detector with Meteor Control System) was used. The measurements were done by using a 35 kV accelaration voltage and 30 mA current.

3.3.7 Pulsation test

Pulsation test were done by using a Maximator system. Three different pressure levels of 3600, 3800, 4000 bar were selected. Test cycles between 10 and 12 million with a application rate of 15 Hz were used since a safety factor of 1.5 is required. After the tests fracture analysis was done by metallographic analysis.

4. RESULTS AND DISCUSSION

4.1 High Pressure Connector

As described in the experimental section, first controlled nitriding trials were conducted on high pressure connector fabricated from quenched and tempered 42CrMo4 steel.

4.1.1 Dependence of the structure, composition and hardness of the nitride layer on nitriding parameters

Because of the gas flow differences inside of the industrial furnace between internal and external part of the HPC, different diffusion and compound layer thicknesses were expected. Thus, inside and outside of the components were evaluated individually.

4.1.1.1 Diffusion and compound layer thicknesses external surface of the HPC

Compound layer and diffusion layers were investigatedby Optical Microscope (OM) and Scanning electron microscope (SEM). Because of existing two different structure which are α-Fe (diffusion layer) and γ'-Fe_4N_{1-x} (compound layer) two different etchants which was mentioned in Section 3.3.1 was used. Klemms-I was used for etching compound layer and Adler for diffusion layer. Because of the complex shape of the components, an uneven distribution of compound layer thickness was observed. Thus the minimum and maximum values of the compound layer are given in Figure 4.3.

An example of optical microscope image of compound layer and diffusion layer on the outside of the samples for first trial series are shown in Figure 4.1.

In case where the compound layer is very thin samples were investigated with SEM. An example of cross sectional SEM image is given in Figure 4.2.

External thickness of diffusion and compound layer of the part nitride under different conditions are given in Figure 4.3 and 4.4.

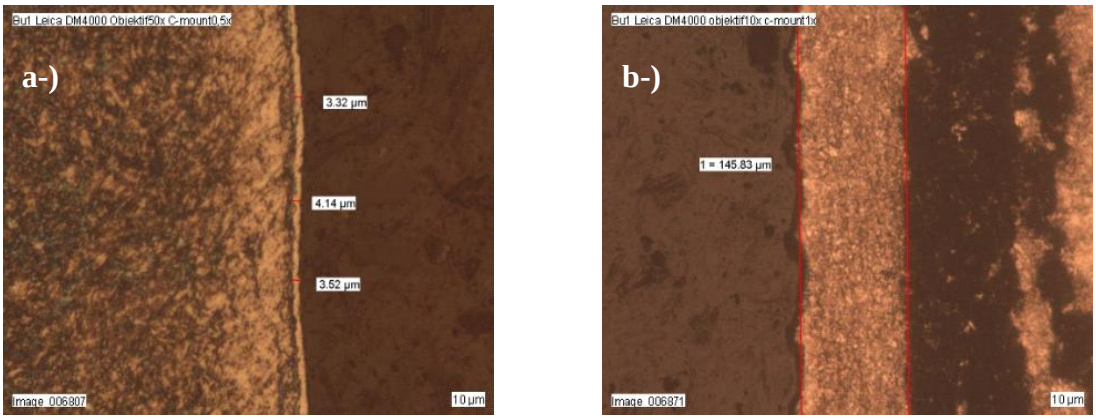

Figure 4.1 : Optical microscope image of nitrided sample
a)CL-outside, (etching with Klemms-I), b)DL-outside
(etching with Adler) (nitriding at 500°C-10h, K_N:0.40)

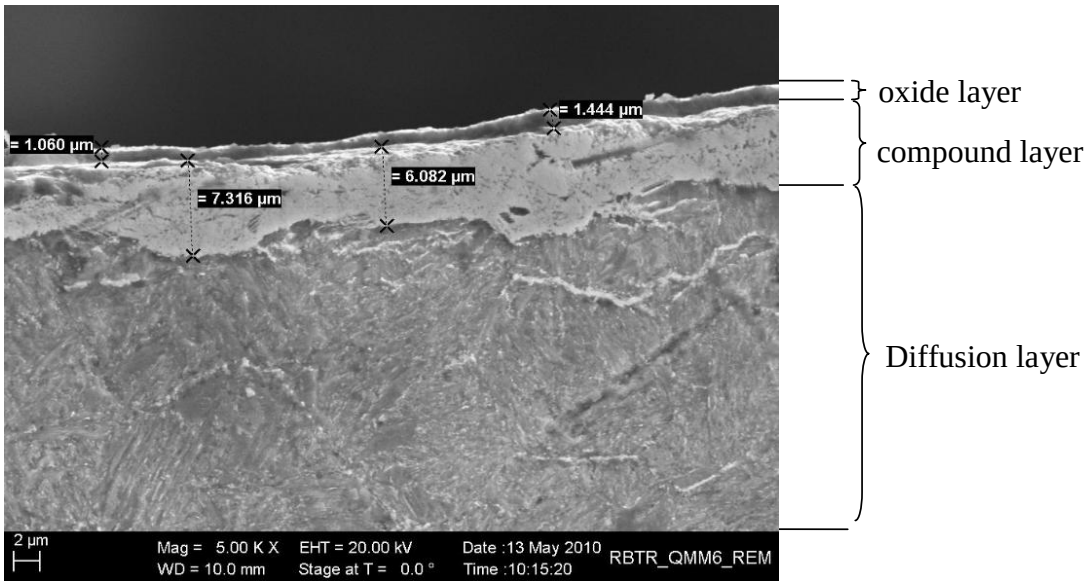

Figure 4.2 : Micro structure of compound layer in SEM

It is seen from the Figure 4.3 and 4.4 that compound and diffusion layer thicknesses increase in parallel to the nitriding duration. And also there is differences between minimum and maximum compound layer thicknesses which is related homogenity of flow rate and activation of surface.

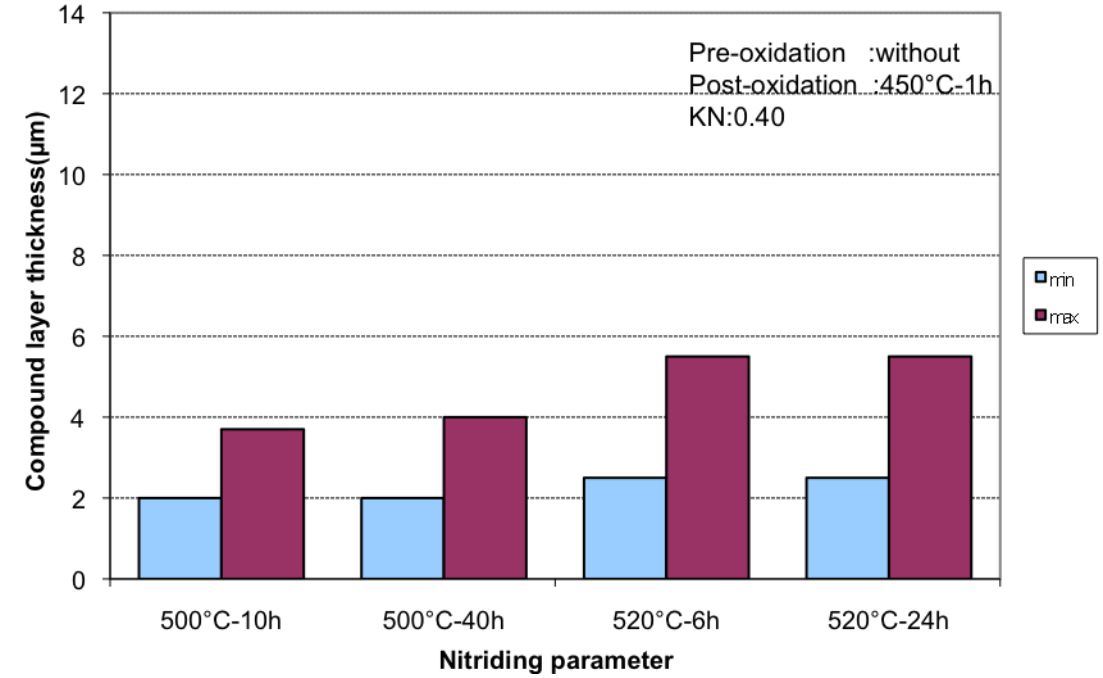

Figure 4.3 : Compound layer distribution external of high pressure connector

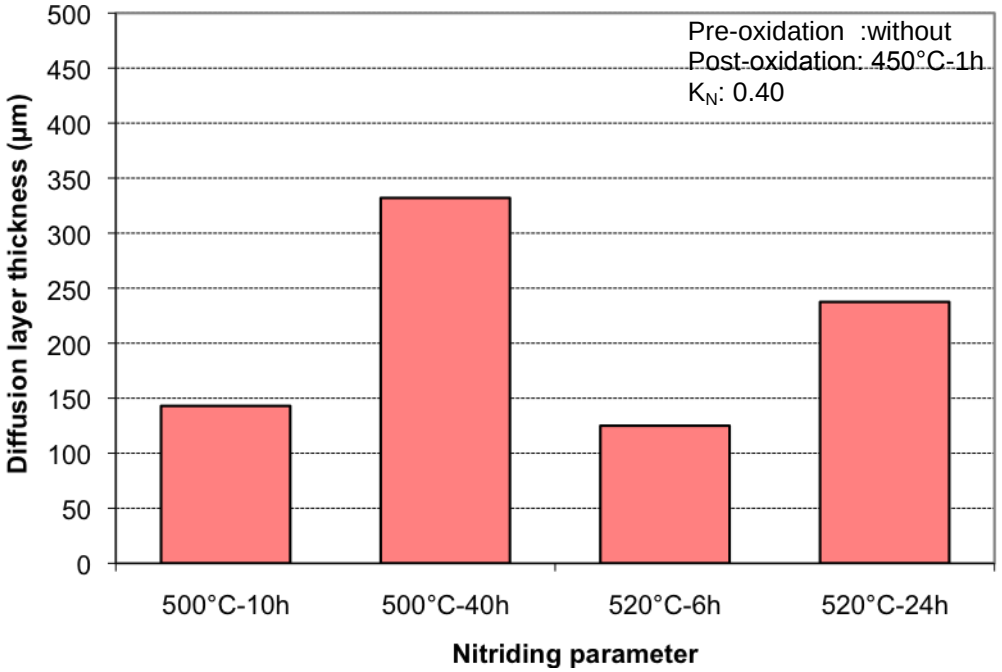

Figure 4.4 : Diffusion layer distribution external of high pressure connector

4.1.1.2 Diffusion and compound layer thicknesses internal surface of the HPC

Diffusion and compound layers on the inside of the HPC were investigated like outside of the HPC. An example of optical microscope image of compound layer and diffusion layer on the inside of the samples for first trial series are shown in Figure 4.5.

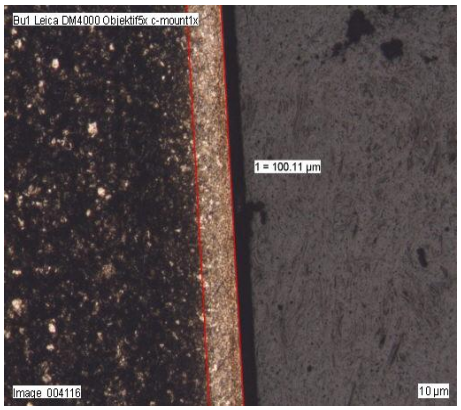

Figure 4.5 : Optical microscope image of nitrided sample DL-inside (etching with Adler) (nitriding at 500C-10h, K_N:0.40)

As expected there were seen differences on thickness of diffusion and compound layer inside of HPC. Distributions of thicknesses depending on nitriding parameters can be seen from Figure 4.6 and 4.7.

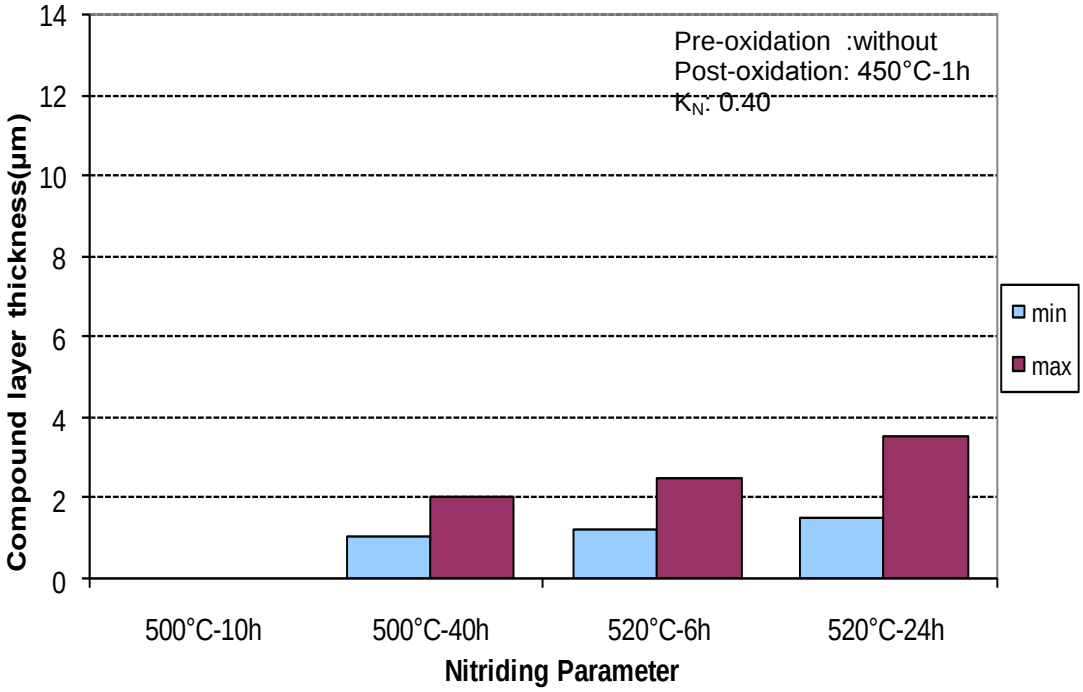

Figure 4.6 : Compound layer distribution on the internal of HPC

It is seen from the Figure 4.6 and 4.7 that compound and diffusion layer thicknesses increase by nitriding duration similarly outside of the HPC. However in this case both compound and diffusion layer thickness are lower due to limited gas flow within the bore.

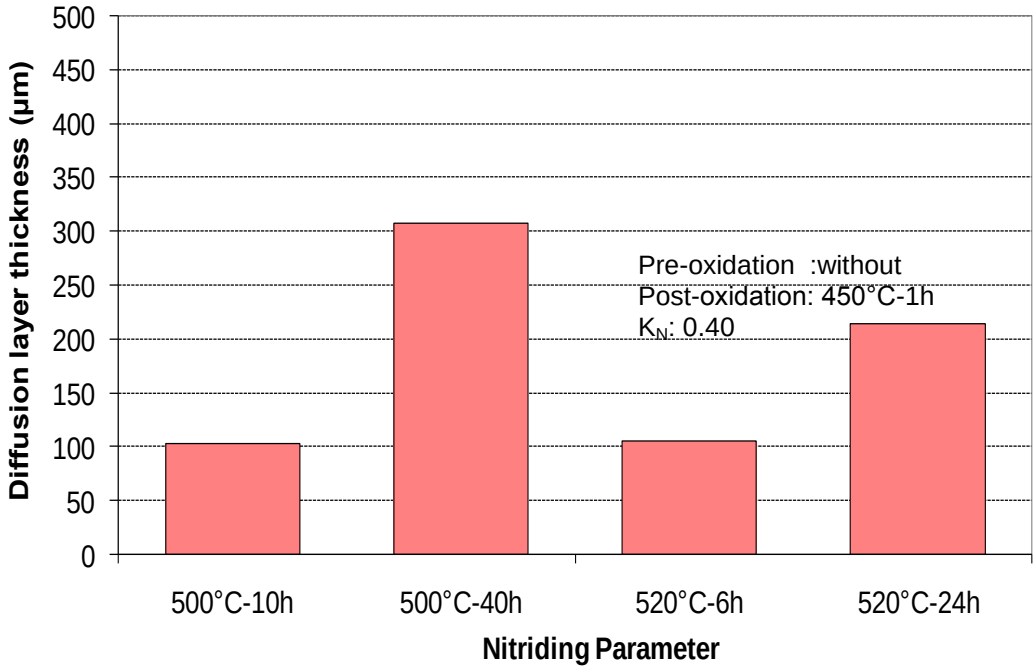

Figure 4.7 : Diffusion layer distribution on the internal of HPC

4.1.1.3 Hardness of high pressure connector

All components have bore holes. Therefore, hardness measurements were performed from both side of the components (Fig. 4.8). Ten measurement points for each trial. The measuring step is 0,05 mm from 0,05 to 0,5 mm.

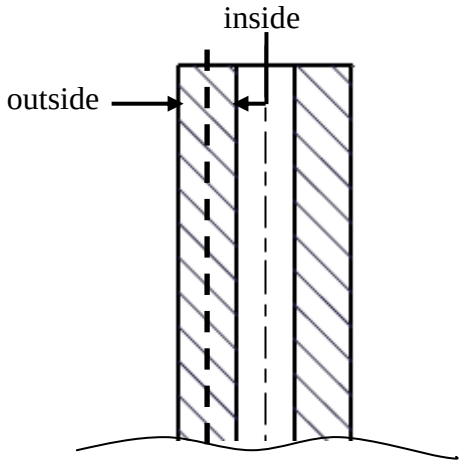

Figure 4.8 : Hardness measurement denominations

Hardness of external and internal side of the HPC can be seen from Figure 4.9 and 4.10.

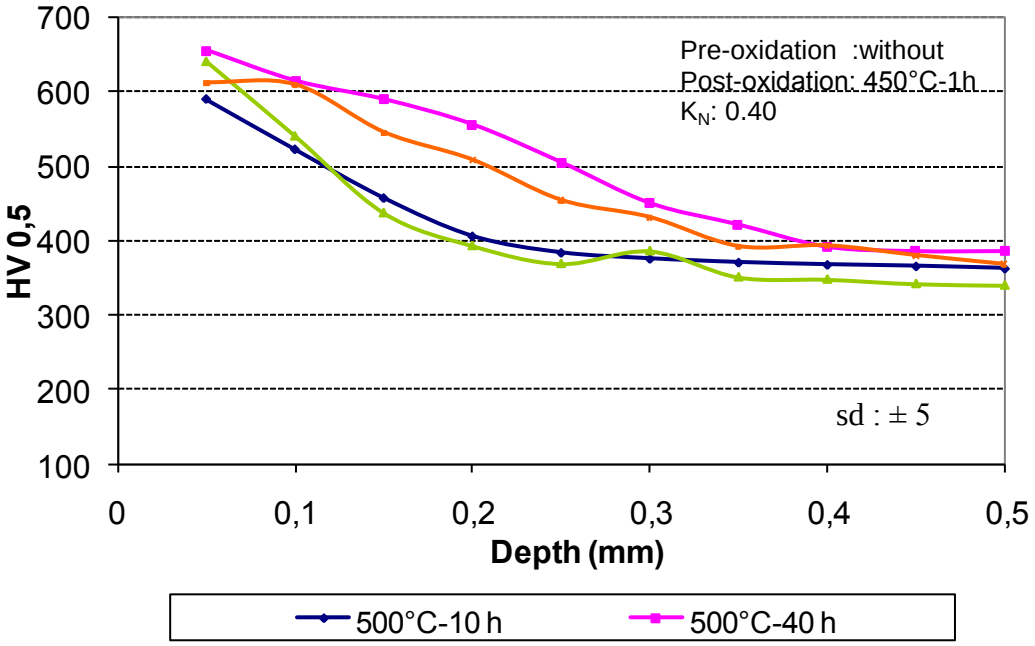

Figure 4.9 : Hardness of external side of HPC

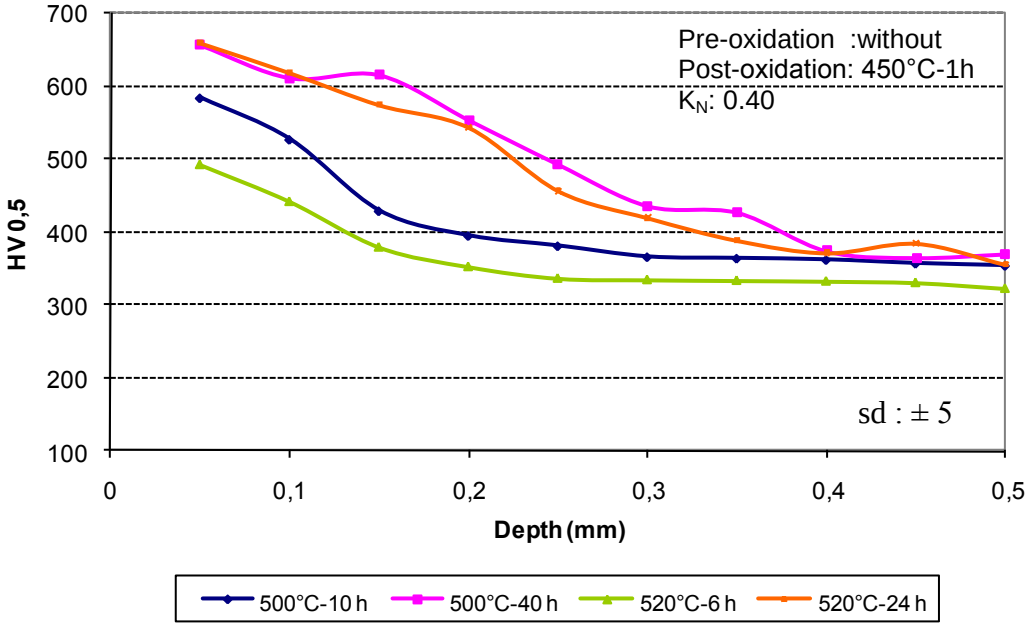

Figure 4.10 : Hardness of internal side of HPC

As seen from the figures, surface near hardness (at 0,05 mm) are more effected from nitriding parameter. Differences on Internal and external hardness values are more visible at short term nitriding process. Nitrided depth can also predicted from hardness-depth curves. They look like similar with metalographic analysis.

4.1.1.4 Concentration-depth profile of HPC

Concentration-depth profile can be observed with elemental analysis which was investigated by Glow Discharge Optical Emission Spectrometry (GDOES).

Effect of time on compound layer thickness and behaviour was investigated on high pressure connector below (Fig. 4.11).

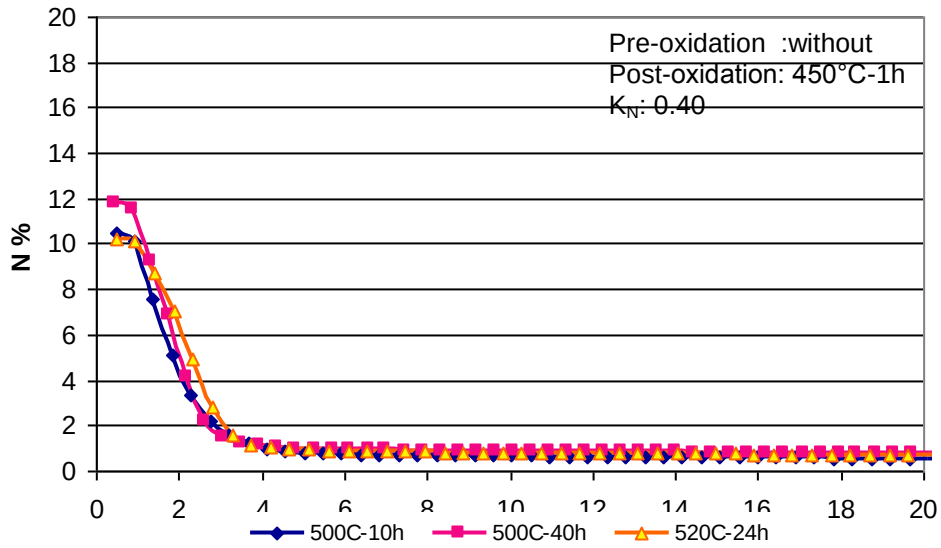

Figure 4.11 : Effect of time on compound layer behaviour on HPC (Material: 42CrMo4)

Concentration-depth profile shows significantly increase of nitrogen concentration near surface reagion which occurs compound layer. However, it is not observed significant nitrogen concentration differences along the diffusion layer. Therefore, only compound and oxide layer behaviour was investigated by GDOES.

GDOES investigation was examined only on the external surface of HPC because of necessariy of flat surface in this measurement technique.

It is seen from the Figure 4.11 that concentration profiles depending on different nitriding parameters shows similar behaviour.

Compound layer thicknesses are not defined from GDOES profiles. Since GDOES measurement is effected from surface roughness and so it is not compatible with metalographic investigation. Thus, compound and diffustion layer thicknesses were determined with metalographic investigations.

4.2 Common Rail (CR) Injector

As described in the experimental section, second controlled nitriding trials were conducted on CR-Injectors fabricated from quenched and tempered 50CrMo4 steel.

4.2.1 Dependence of the structure, composition and hardness of the nitride layer on nitriding parameters

As mentioned at the beginning of the first trial series, inside and outside of the CR-Injector were also evaluated individually like HPC because of gas flow differences inside of the industrial furnace.

4.2.1.1 Diffusion and compound layer thicknesses external surface of the CR-injector

After the first trails which had conducted by high pressure connector, there were proceeded trials with CR-Injector which is main objective to be done nitriding. There were selected best nitriding parameter which was 520°C with one hour uncontrolled nitriding and five hours controlled nitriding with K_N 0,40 by getting experience from fatigue strength of HPC which was explained in Section 4.5.

External thickness of diffusion and compound layer of the part can be seen from Figure 4.12 and 4.13.

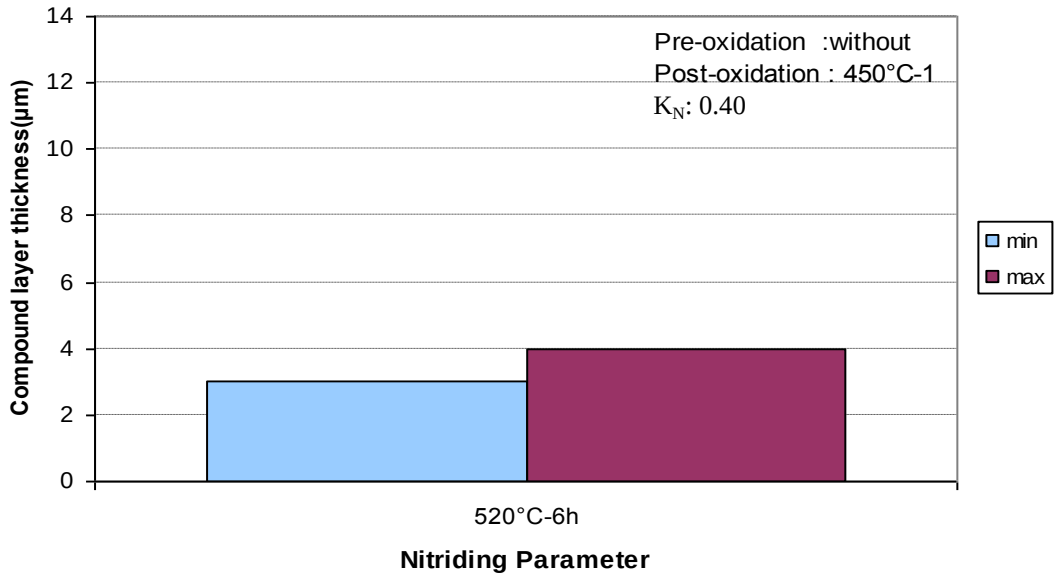

Figure 4.12 : Compound layer distribution on the external of CR-Injector

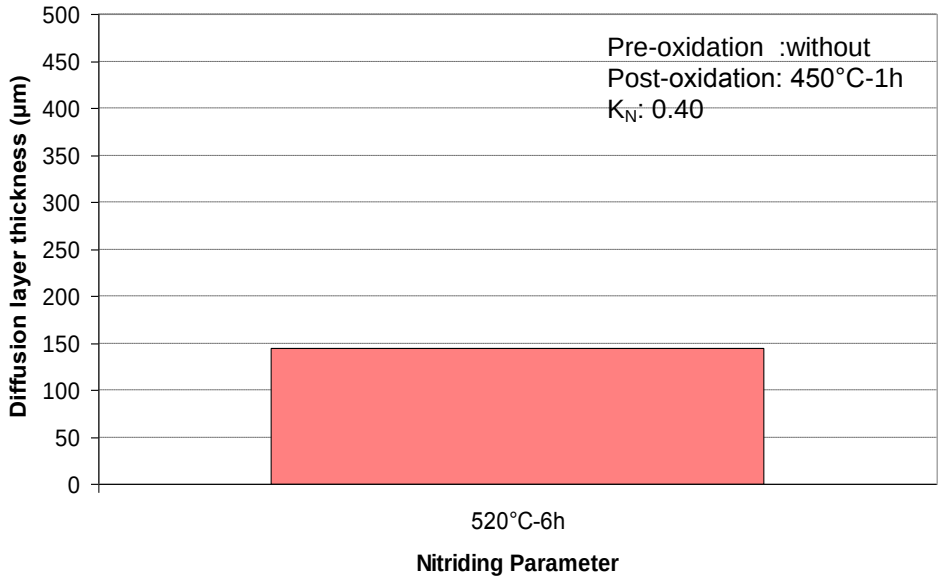

Figure 4.13 : Diffusion layer distribution on the external of CR-Injector

Comparison of external thickness of HPC and CR-Injector shows similar layer thickness.

4.2.1.2 Diffusion and compound layer thicknesses internal surface of the CR-injector

Internal thickness of diffusion and compound layer of the part can be seen from Figure 4.14 and 4.15.

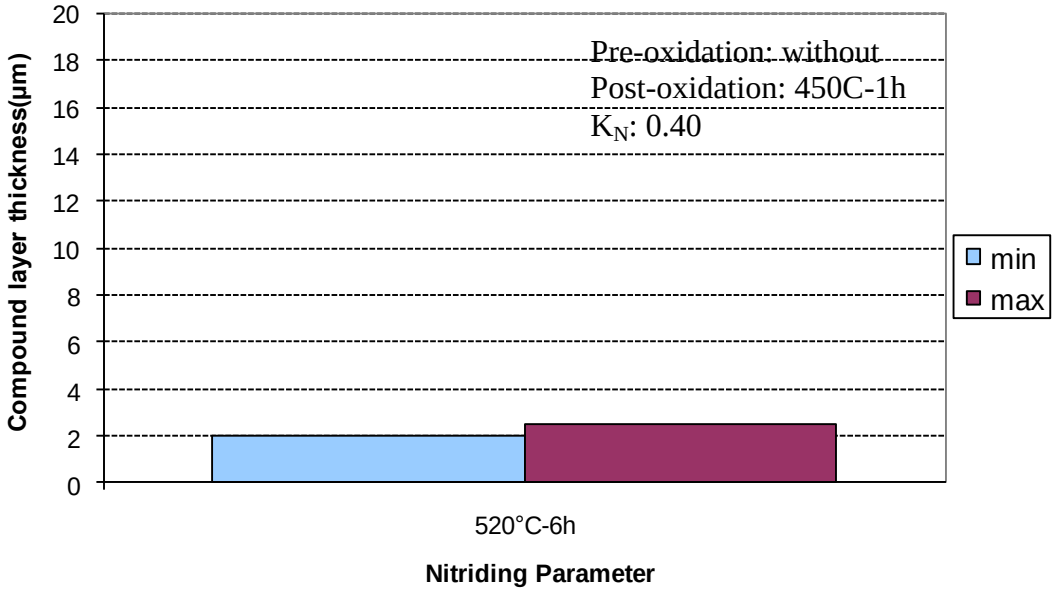

Figure 4.14 : Compound layer distribution on the internal of CR-Injector

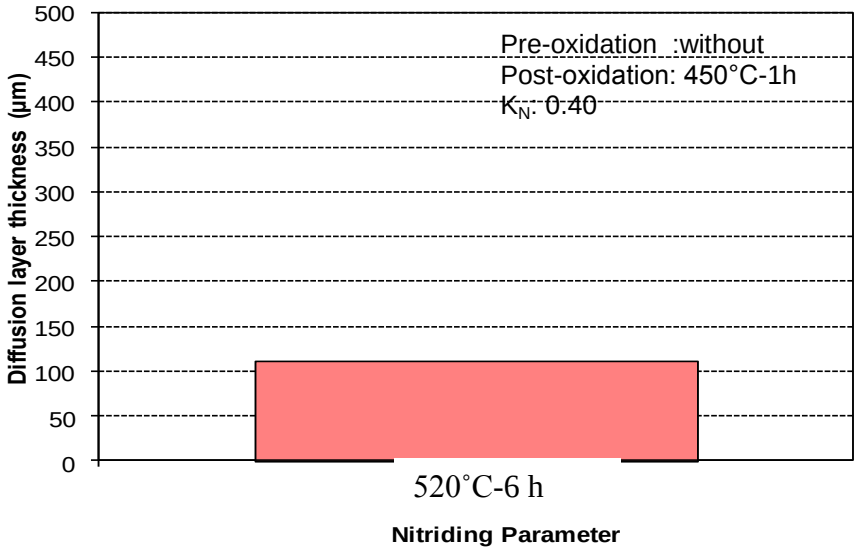

Figure 4.15 : Diffusion layer distribution on the internal of CR-Injector

As seen from the Figure 4.14 and 4.15, there are differences between internal and external side of CR-Injector because of gas flow and surface quality.

4.2.1.3 Hardness of common rail injector

Hardness investigations were examined like high pressure connector which was mentioned in Section 4.1.2.3 and according to directions in Section 3.3.2. Hardness-depth profile in the external and internal of the CR-Injector are seen in Figure 4.16.

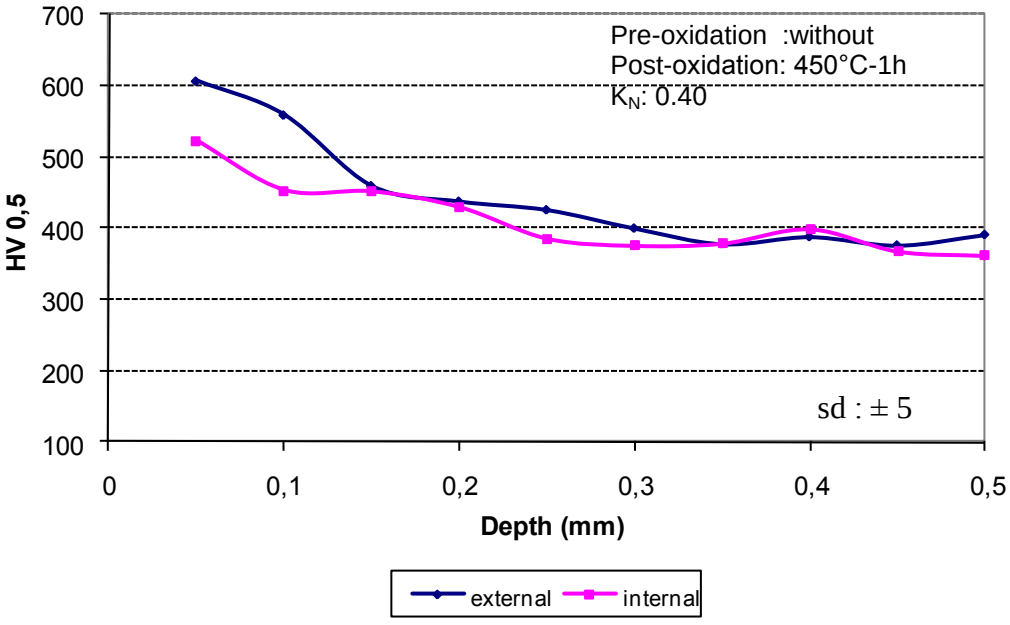

Figure 4.16 : Hardness of external and internal side of CR-Injector

As expected and also it is showed by diffusion layer thickness, internal surface near hardness is lower than external surface near hardness because of gas flow distrubition inside of the furnace.

Comparison of hadnesses between HPC and CR-Injector shows similarity.

4.2.1.4 Concentration-depth profile of common rail injector

Concentration profile along CR-Injector is seen from Figure 4.17. Uncontrolled nitriding time and temperature are effected to compound layer behaviour. Along invard diffusion behaviour of nitrogen shows smaller acceleration.

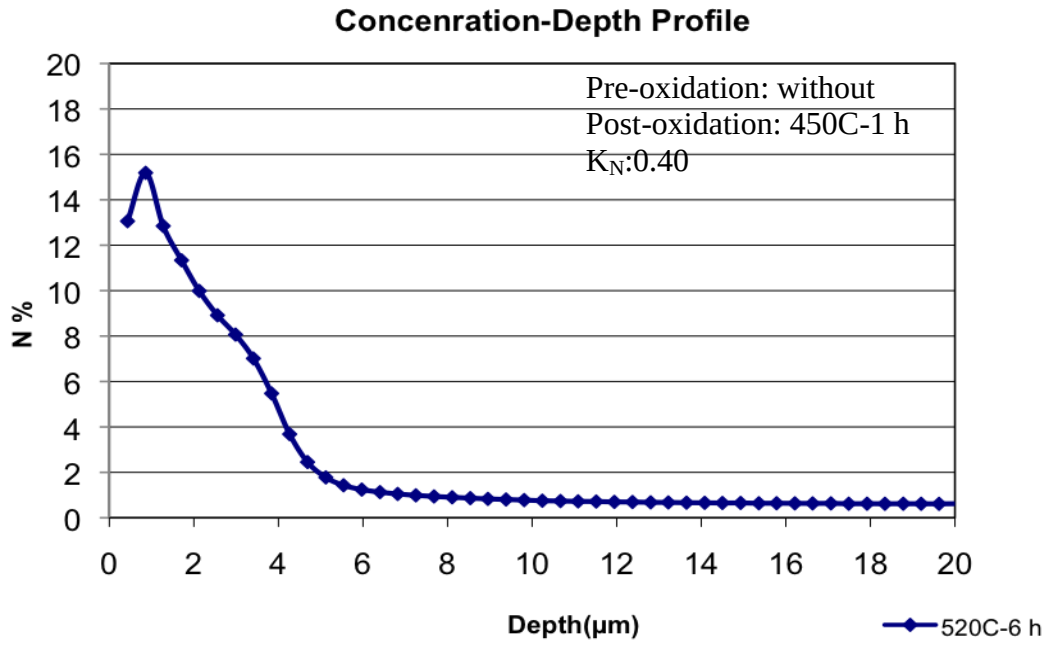

Figure 4.17 : Effect of temperature on compound layer behaviour (Material:50CrMo4)

From the Figure 4.17, nitrogen concentration increases along the oxide layer which is below 1 µm shows. After 1 µm compound layer has started to be seen and nitrogen concentration started to decrease with high slope along compound layer thickness.

4.3 Though Hole Sample

As described in the experimental section, third controlled nitriding trials were conducted on through hole samples fabricated from quenched and tempered 50CrMo4 steel.

4.3.1 Dependence of the structure, composition and hardness of the nitride layer on nitriding parameters

Beside the nitriding parameter of 520°C-6 h which was examined for HPC and CR-Injector, three different nitriding parameters were also used to compare effect of pre and post oxidation treatments on nitriding parameters.

Inside and outside surface of samples were examined individually similar to other components.

4.3.1.1 Diffusion and compound layer thicknesses external surface of the through hole samples

After the first and second trial series with high pressure connector and CR-Injector to get optimum parameter for fatigue strength, through hole samples are used mainly for improving homogenity of compound layer and corrosion resistance with pre and post oxidation treatments. Three pre-oxidation and three post-oxidation parameters were defined (Table 3.4).

Distributions of diffusion and compound layer thicknesses external side of bore trought samples depending on nitriding, pre-oxidation and post-oxidation parameters can be seen from Figure 4.18 and 4.19.

It is seen from Figure 4.18 that minimum and maximum compound layer thickness are closer each other because of pre-oxidation treatment which supplies activation of the surface. Diffusion layer thickness is not effected from pre-oxidation as much as compound layer thickness.

Within the pre-oxidation parameters, the smallest differences between minimum and maximum compound layer thicknesses were seen with 450°C-1 hour. Also, diffustion layer thickness increased by pre-oxidation treatment with 450°C-1 hour.

Comparison of the pre-oxidation parameters show that, relatively low temperatures (350°C and 450°C) with less treatment duration give better layer quality and thickness.

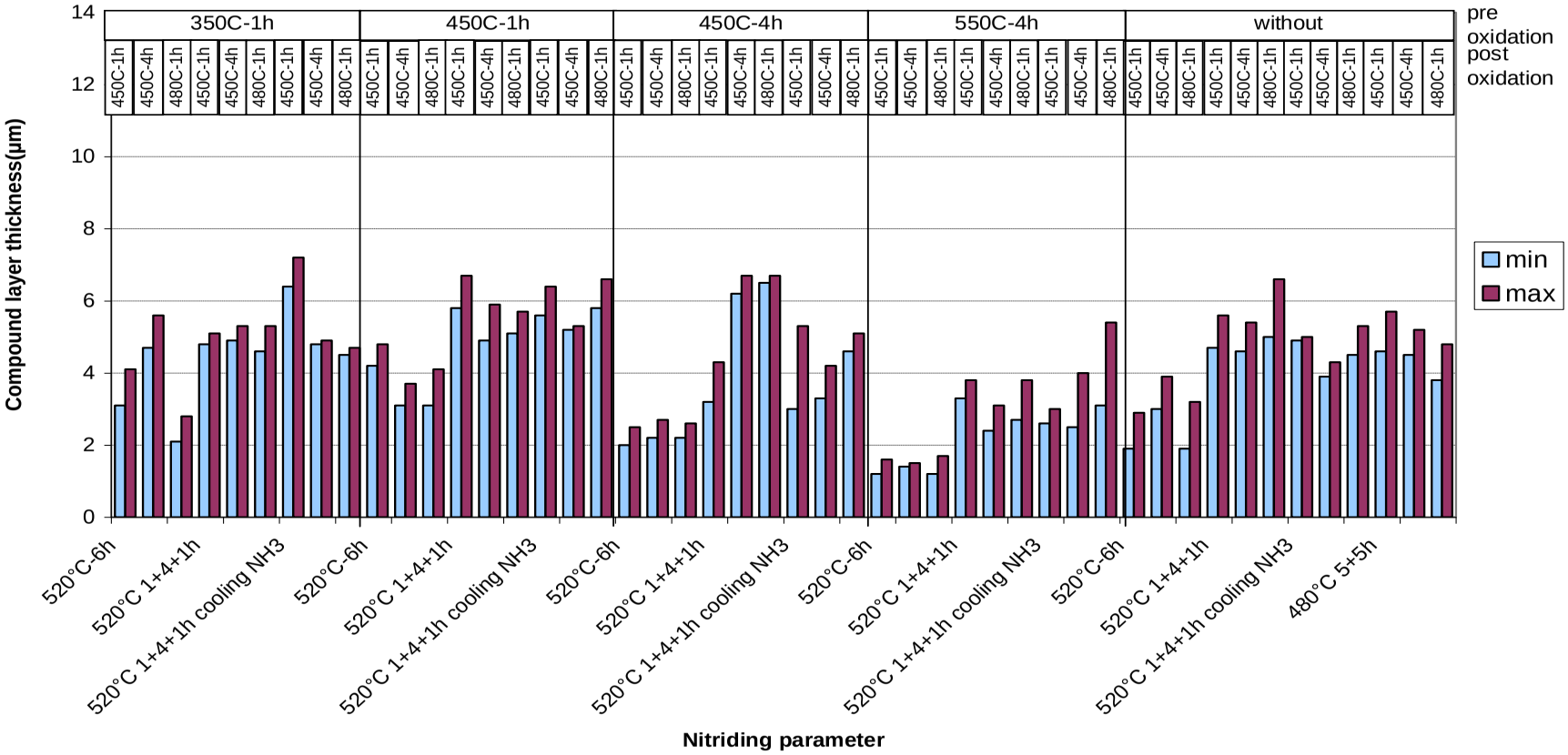

Figure 4.18 : Compound layer distribution on the external of THS

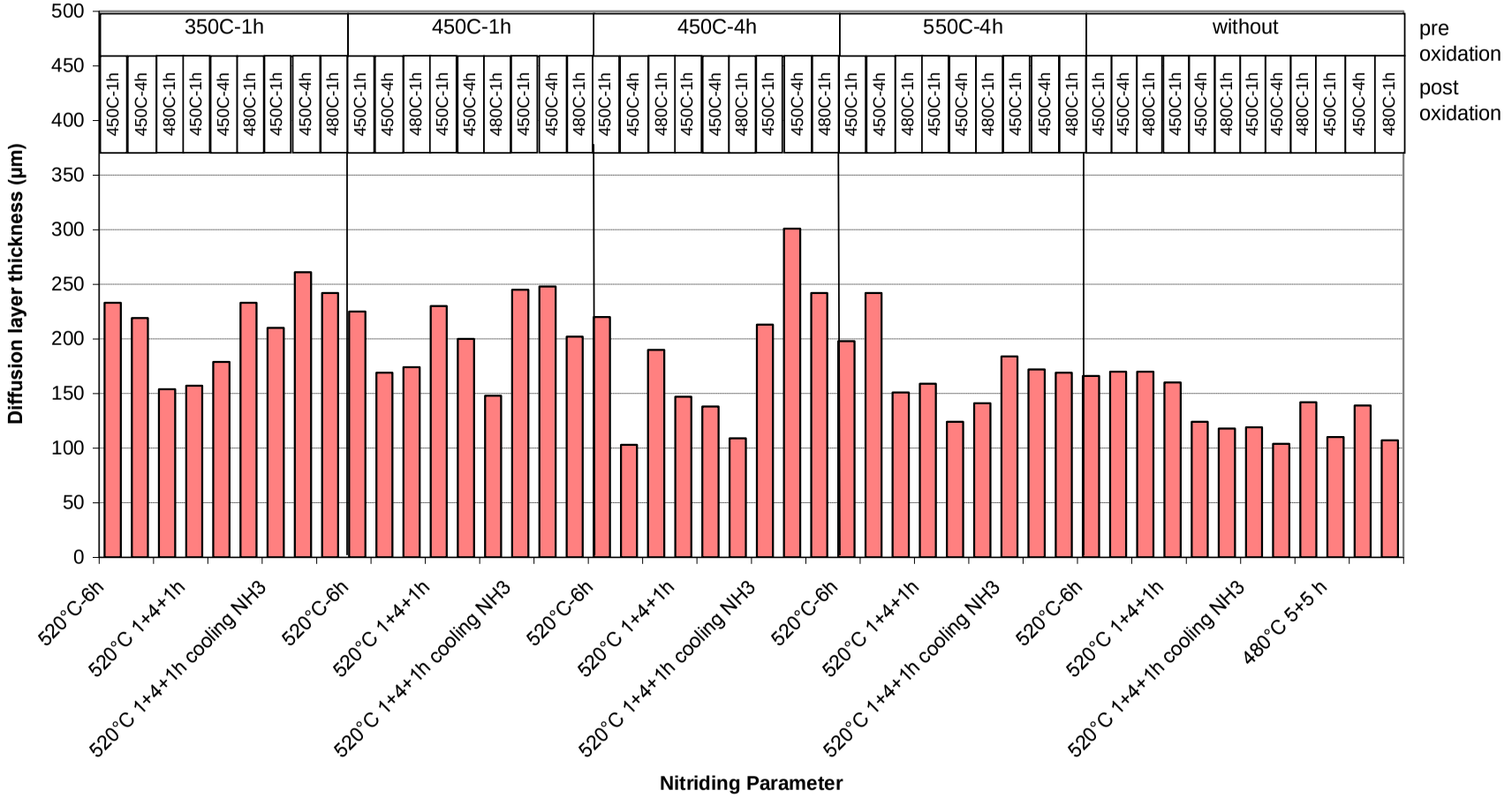

Figure 4.19 : Diffusion layer distribution on the external of THS

4.3.1.2 Diffusion and compound layer thicknesses internal surface of the through hole samples

Distributions of diffusion and compound layer thicknesses external side of through hole samples depending on nitriding, pre-oxidation and post-oxidation parameters can be seen from Figure 4.20 and 4.21.

Diffusion layer thickness are more important internal surface of component for fatigue strength. Thus, pre-oxidation with 450°C shows higher diffusion layer thickness. However, if it is compared with also compound layer thickness quality, 450°C-1 hour achives best results.

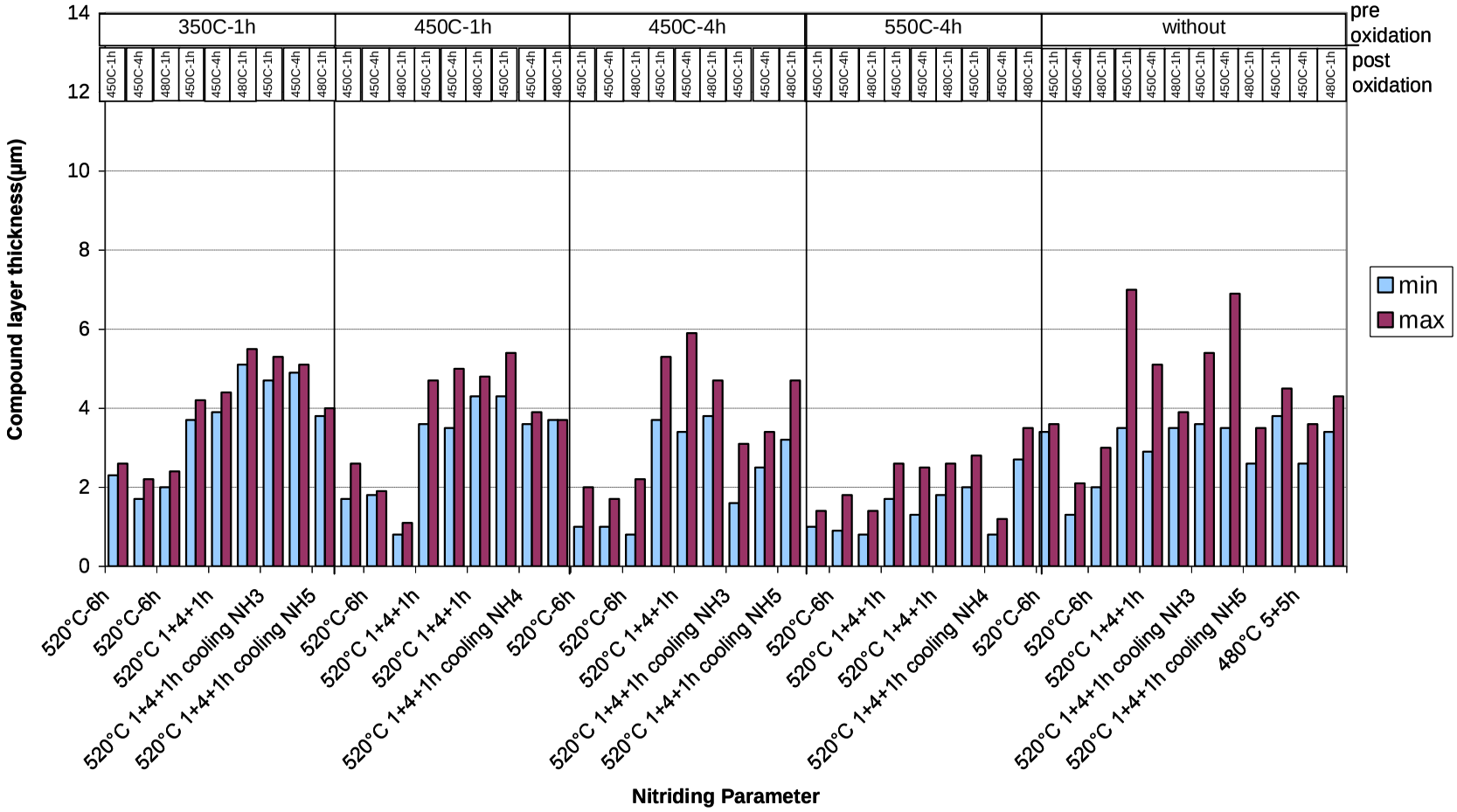

Figure 4.20 : Compound layer distribution on the internal of THS

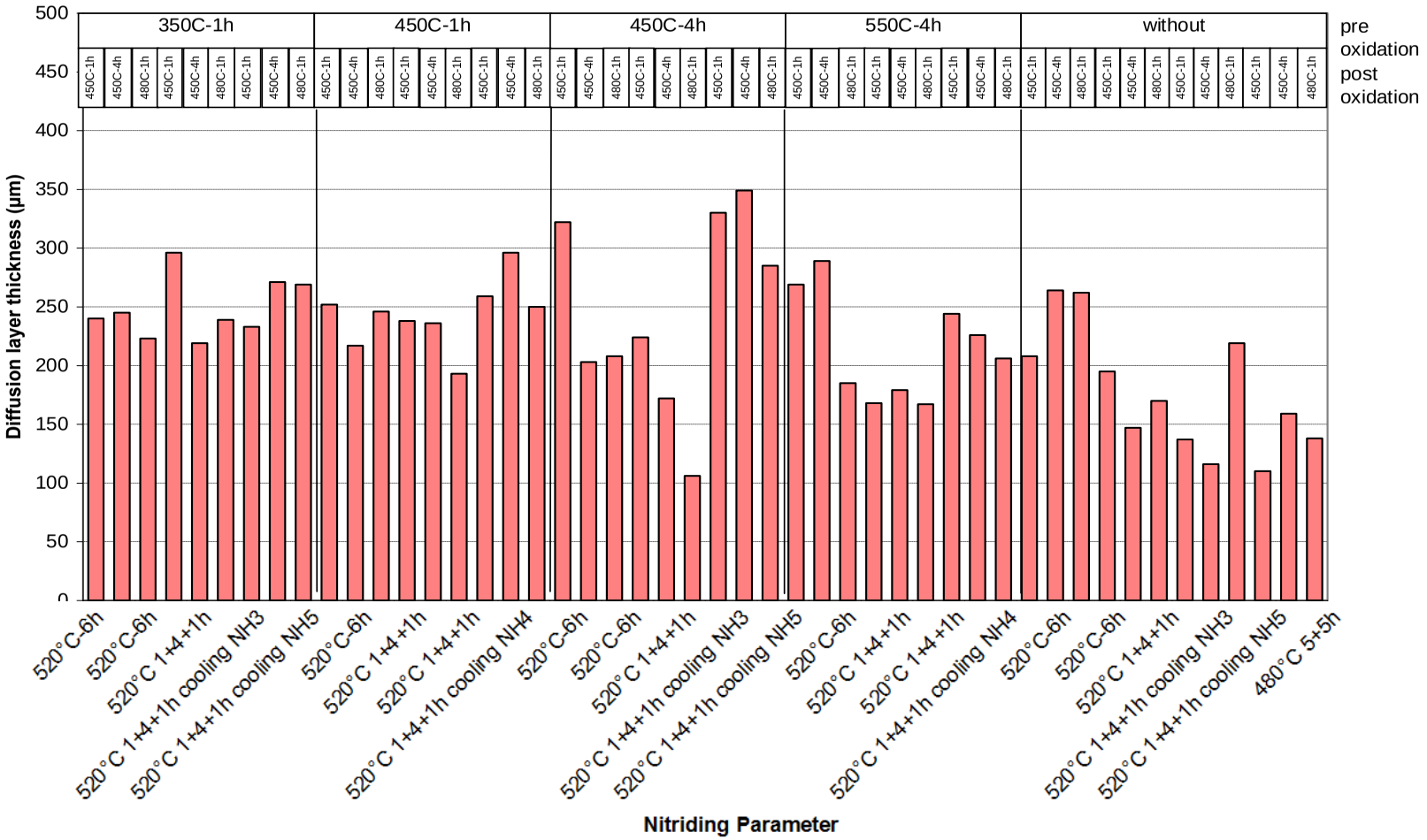

Figure 4.21 : Diffusion layer distribution on the internal of THS

4.3.1.3 Hardness of through hole samples

Hardness measurements were examined like HPC and CR-Injector and according to directions which was mentioned section 3.3.2.

Hardness distributions external nad internal side of the samples in 0,05 mm and 0,5 mm can be seen in Figure 4.22 and 4.23.

Pre and Post oxidation treatments are not effected on surface near hardness. Diffrences of surface hardness was caused because of nitriding parameters.

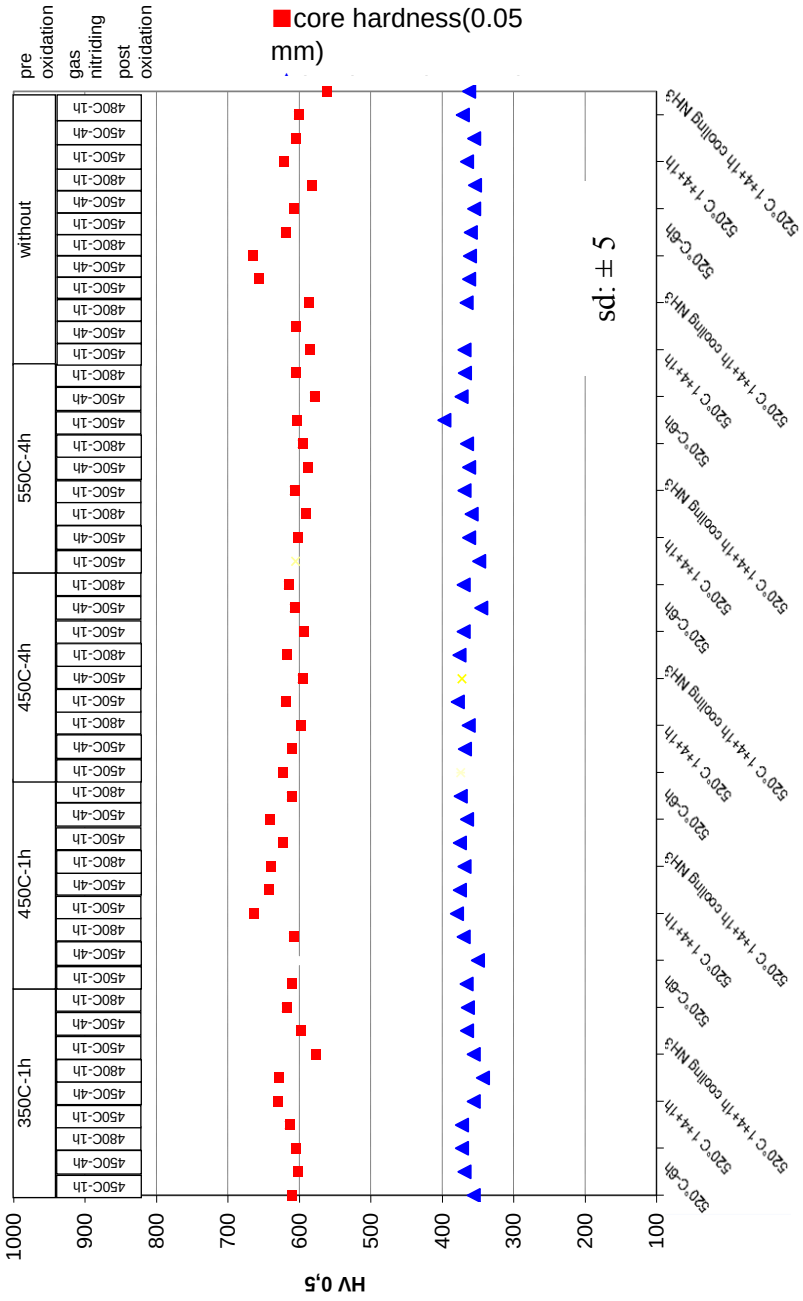

Figure 4.22 : Hardness on the external of THS

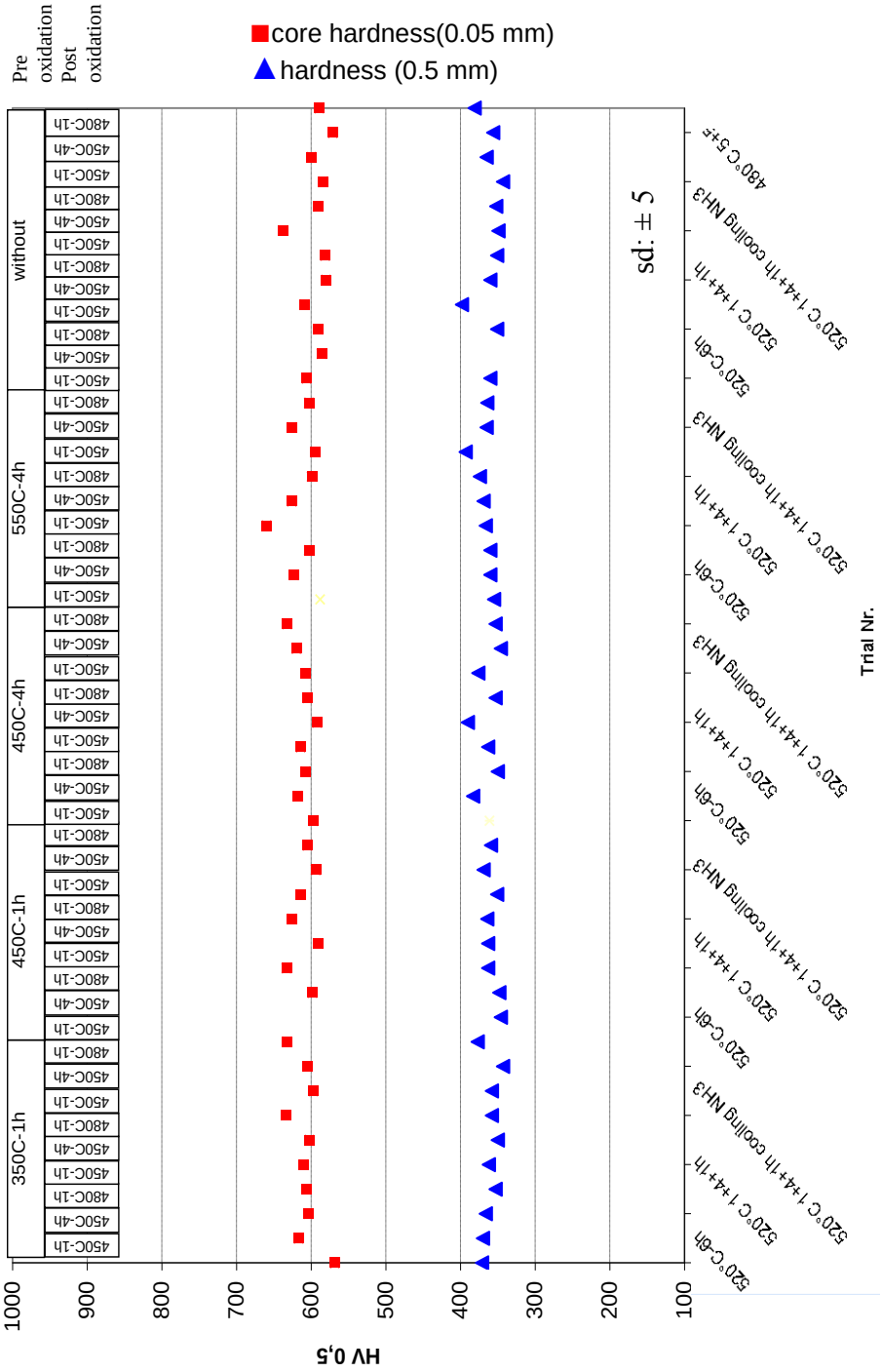

Figure 4.23 : Hardness on the internal of THS

4.3.1.4 Concentration-depth profile of through hole samples

As mentioned before preoxidation treats surface activation of nitriding so there is obtained more homogeneous compound layer. These measurements were only conducted in order to see the effect of pretreatment time and temperature on the compound layer thickness (Fig. 4.24)

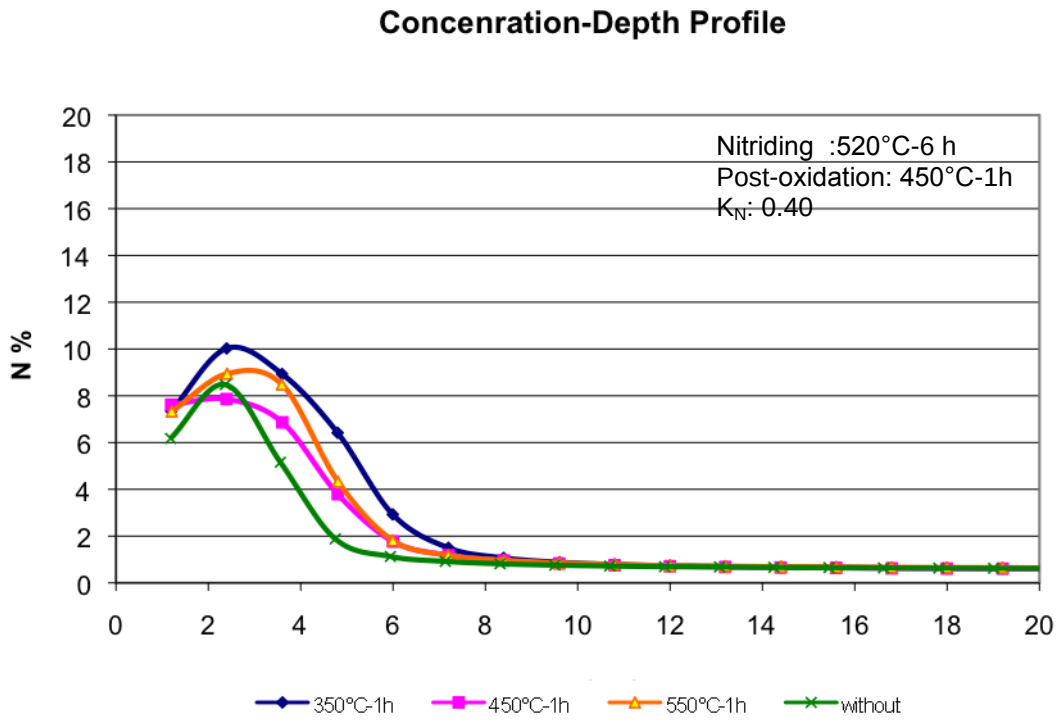

Figure 4.24 : Effect of pre-oxidation parameters on compound layer behaviour (Material: 50CrMo4)

The results of these measurments further supported the increase of compound layer thickness with the pre oxidation process.

Relying on the positive effcet of pre oxidaiton on the compound alayer homogenity preoxidized samples are subjected to post oxidation for improving the corrosion resistance.

Effect of post-oxidation parameters on compound layer behaviour was compared in Figure 4.25. It was occurred black oxide by post-oxidation with water which it was magnetit phase on the compound layer at these temperatures (450°C, 480°C). Oxide layer behaviour below 1 µm was not investigated because of GDOES sensibility but after 1 µm oxygen concentration behaviours show similar behaviour in both of post-oxidation parameters (dashed lines).

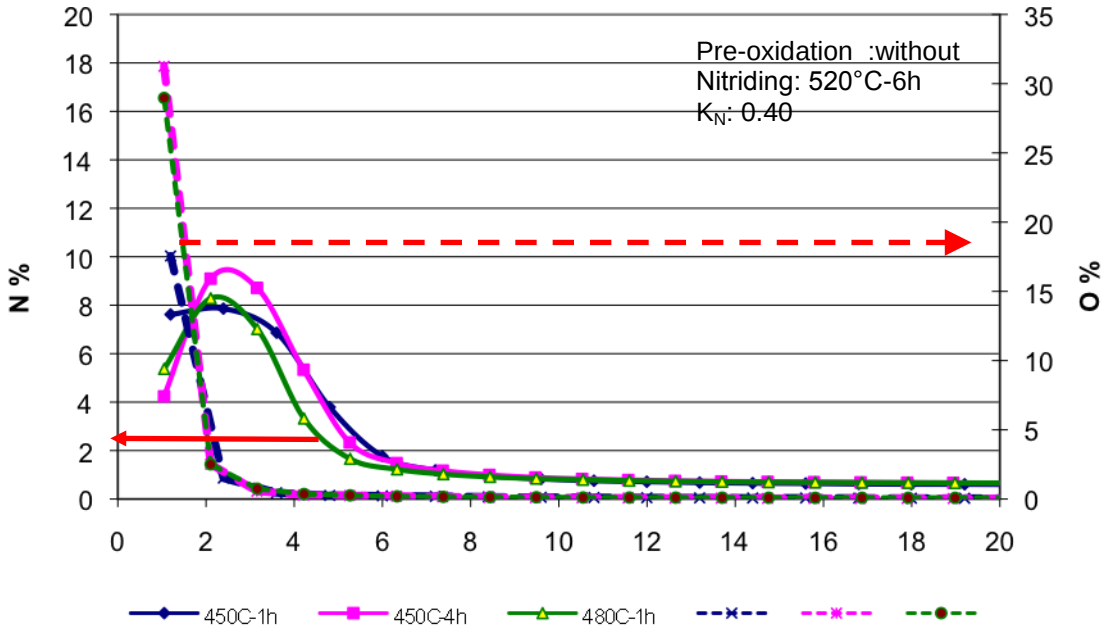

Figure 4.25: Effect of post-oxidation parameters on compound layer behaviour (Material: 50CrMo4)

4.4 Corrosion Resistance of Components

Corrosion resistance were investigated only outside of the components because there needed to be cut the parts to evaluate inside of the components which were made mistake for evaluation. They were tested by salt spray test to evaluate effect of post-oxidation treatment beside nitriding. Corrosion tests were proceed 5,5 h according to DIN EN ISO 9227:2006. It is seen that unnitrided high pressure connector (Fig. 4.26-a) was evaluated as a Ri5 and nitrided+post-oxidation high pressure connector was evaluated as a Ri2 according to 10DIN EN ISO 4628-3:2003. They also were compared with other corrosion protection coating which is phospating (Fig. 4.26-b). Nitriding with post-oxidation showed better results than phosphated sample (Fig. 4.26-d).

Salt spray test were done with twelve samples in one test duration (5,5 h). It is seen from Figure 4.27 that all samples were achieved Ri3 and below.

Distribution of corrosion pittings are seen in Figure 4.28-4.29-4.30.

Figure 4.26 : Corrosion test results a)unnitrided, b)phospated, c)nitrided(520°C-6h),d)pre-oxidaized+nitrided+post oxidation(450°C-1 h)

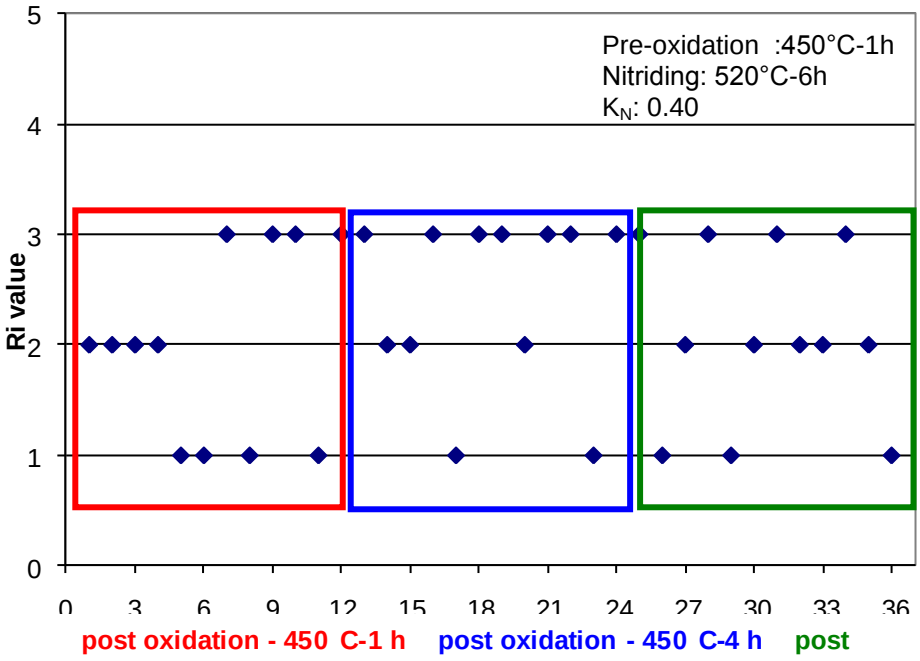

Figure 4.27 : Salt spray test evaluation results for different post-oxidation parameters

520°C-(1+4+1+cooling NH3)h

520°C-(1+4+1)h

520°C-(1+5)h

520°C-(1+4+ 1+cooling NH3)h

520°C-(1+4+1)h

520°C-(1+5)h

520°C-(1+4+ 1+cooling NH3)h

520°C-(1+4+1)h

520°C-(1+5)h

520°C-(1+4+ 1+cooling NH3)h

520°C-(1+4+1)h

520°C-(1+5)h

Figure 4.28 : Corrosion test results for nitrided with post-oxidation (450°C-1 h)

520°C-(1+4+ 1+cooling NH3)h

520°C-(1+4+1)h

520°C-(1+5)h

520°C-(1+4+ 1+cooling NH3)h

520°C-(1+4+1)h

520°C-(1+5)h

520°C-(1+4+ 1+cooling NH3)h

520°C-(1+4+1)h

520°C-(1+5)h

520°C-(1+4+ 1+cooling NH3)h

520°C-(1+4+1)h

520°C-(1+5)h

Figure 4.29 : Corrosion test results for nitrided with post-oxidation (450°C-4 h)

520°C-(1+4+1+ cooling NH3)h

520°C-(1+4+1)h

520°C-(1+5)h

520°C-(1+4+ 1+cooling NH3)h

520°C-(1+4+1)h

520°C-(1+5)h

520°C-(1+4+ 1+cooling NH3)h

520°C-(1+4+1)h

520°C-(1+5)h

520°C-(1+4+ 1+cooling NH3)h

520°C-(1+4+1)h

520°C-(1+5)h

Figure 4.30 : Corrosion test results for nitrided with post-oxidation (480°C-1 h)

4.5 Residual Stress, Fatigue Resistance and Fracture Analysis

4.5.1 Residual stress analysis of high pressure connector

As mentioned before residual stresses are very critical for fatigue strength. Therefore, there need to be seen residual stress behaviour along nitride layers especially inside of the component because of cyclic load. Residual stress measurements were examined by XRD in Feuerbach/Germany. Residual stress behaviour is shown in Figure 4.31.

Nitriding region shows compressive residual stress behaviour. Compressive residual stress behaviour depends on nitriding duration and temperature which is seen in Figure 4.31. By inward diffusion, compressive residual stress values increase. However, relatively long term nitriding (24 h and 40 h) shows different residual stress behaviour with increasing distance from the surface from short term nitriding (6 h and 10 h). By increasing nitiriding duration compressive residual stress moves along nitride layer.

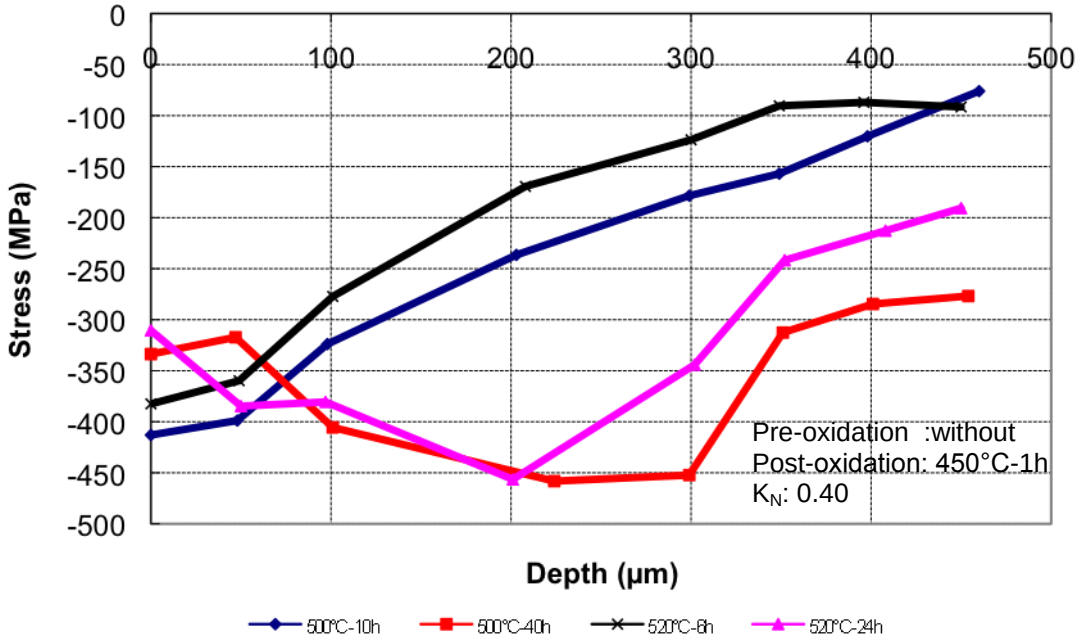

Figure 4.31 : Residual stress behaviour of HPC (Material:42CrMo4)

4.5.2 Fatigue resistance of high pressure connector

Fatigue strength tests were examined in pulsation pressure test machine which was mentioned in Section 3.3.7. Pressure pulsation tests take long time nearly one mounth per test. Therefore, they were done pressure pulsation test for minimum and maximum nitriding duration trials for high pressure connector which are 500°C-40 h and 520°C-6 h. Wöhler diagram can seen form Figure 4.34.

Pressure pulsation test bases on statistical calculation. As a consequence of numerous unrecorded or undetectable factors that affect the fatigue strength of components, the results of fatigue strength tests conducted on identical test specimens or components under identical conditions vary. As a result, statistical evaluation of the pressure pulsation test is necessary in order to obtain permitted pressure level.

The strength of components is subject to statistical variation, see Figure 4.32. Consequently, any statement about the fatigue strength of a component can be made only in conjunction with a specific failure probability. With the aid of the statistical methods described in the following, Wöhler curves associated with specific failure probabilities can be derived from the results of the pressure pulsation test.

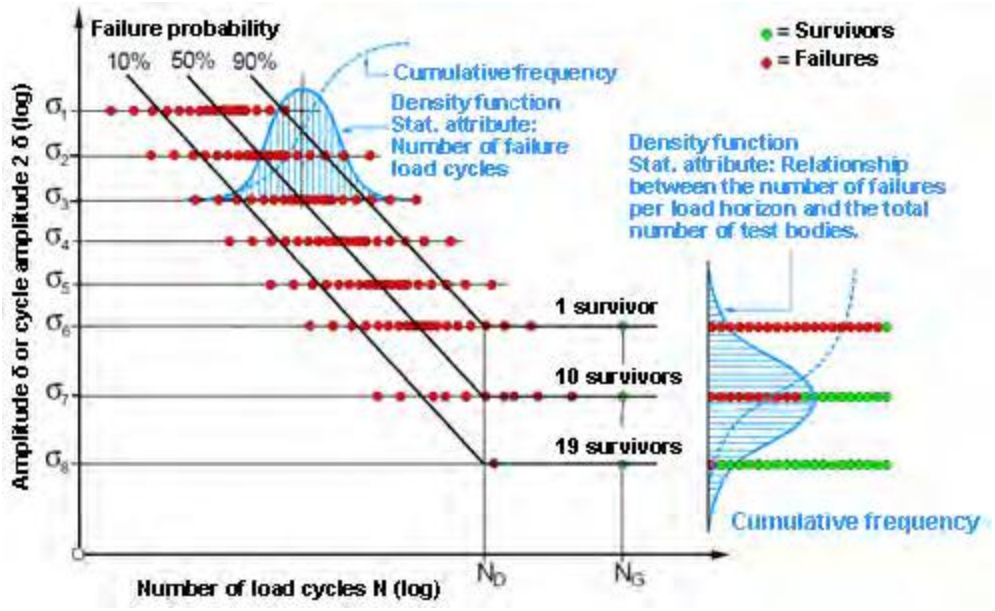

Figure 4.32 : Variation in Pressure pulsation test results, statistical evaluation and Wöhler curves as a function of failure probability

To determine the level with a failure probability of 50%, there must be two bracketing levels. The ratio of the number of failed components r to the total number of components per pressure level n serves as the statistical feature or attribute. From these two quantities and with the aid of the estimation formulas

$$P_f = \frac{3r-1}{3n+1} \qquad \textbf{(4.1)}$$

$$P_f = 0.5^{\frac{1}{n}} \quad for \;\; r = n \qquad \textbf{(4.2)}$$

$$P_f = 1 - 0.5^{\frac{1}{n}} \quad for \;\; r = 0 \qquad \textbf{(4.3)}$$

an associated failure probability is calculated for each pressure level. As an example, Trial 3 (520°C-6h) was mentioned below. The calculated failure probabilities are subsequently plotted against the logarithmic pressure level in the probability graph for the normal distribution, see Fig.4.33

The distribution function appears as a straight line on a probability graph and is determined by means of a least squares fit. The statistical parameters the mean of the sample, the long-term endurance strength ΔpD50% at a failure probability of

Pf = 50% and the variation (dispersion) in the form of the scatter range 1/TS = ΔpD90%/ΔpD10% are calculated with the aid of these regression lines.

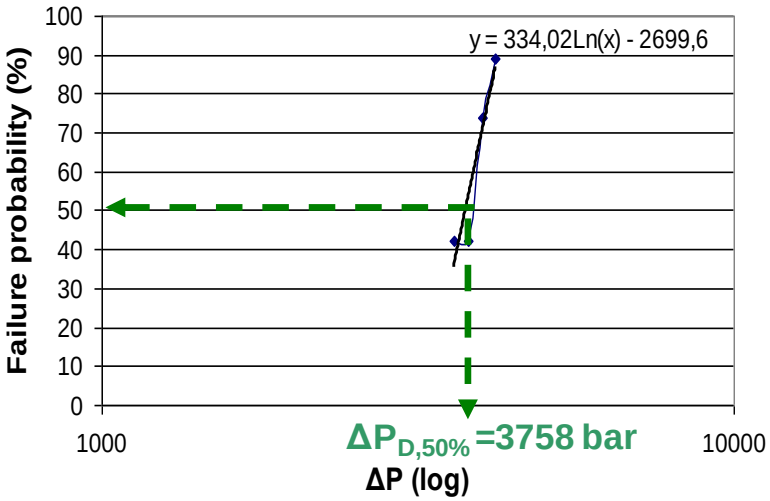

Figure 4.33 : Statistical evaluation by means of a probability graph

The loads and load capacity (fatigue strength) of components are subject to statistical variation that is generally caused by unknown factors. Accordingly, to ensure the fatigue strength of a component with a specific failure probability, a safety factor based on statistics is required. Using this safety factor, it is possible to draw conclusions about the permissible load in service from the long-term endurance strength at a failure probability of Pf = 50%.

When determining the fatigue strength, the variation is generally characterized by the scatter expressed in the form

$$\frac{1}{T_s} = \frac{\Delta P_{D,90\%}}{\Delta P_{D,10\%}} = \frac{4269}{3335} = 1.25 \qquad \textbf{(4.4)}$$

and not by the standard deviation s.

In the case of a log-normal distribution, the standard deviation s can then be calculated specifically as

$$s = \frac{1}{2.56} \log(\frac{1}{T_s}) = 0.038 \qquad \textbf{(4.5)}$$

from the scatter. And safety factor is calculated with normalized attribure value (uo) standart deviation.

$$j_s = 10^{-u_o.s} = 10^{4.75*0.038} = 1.51 \quad \textbf{(4.6)}$$

The maximum permissible pressure occurring in service, including pressure spikes, is obtained as

$$\Delta P_{perm} = \frac{\Delta P_{D,50\%}}{j_S} = \frac{3715}{1.51} = 2460\ bar \quad \textbf{(4.7)}$$

for a fatigue-resisting design.

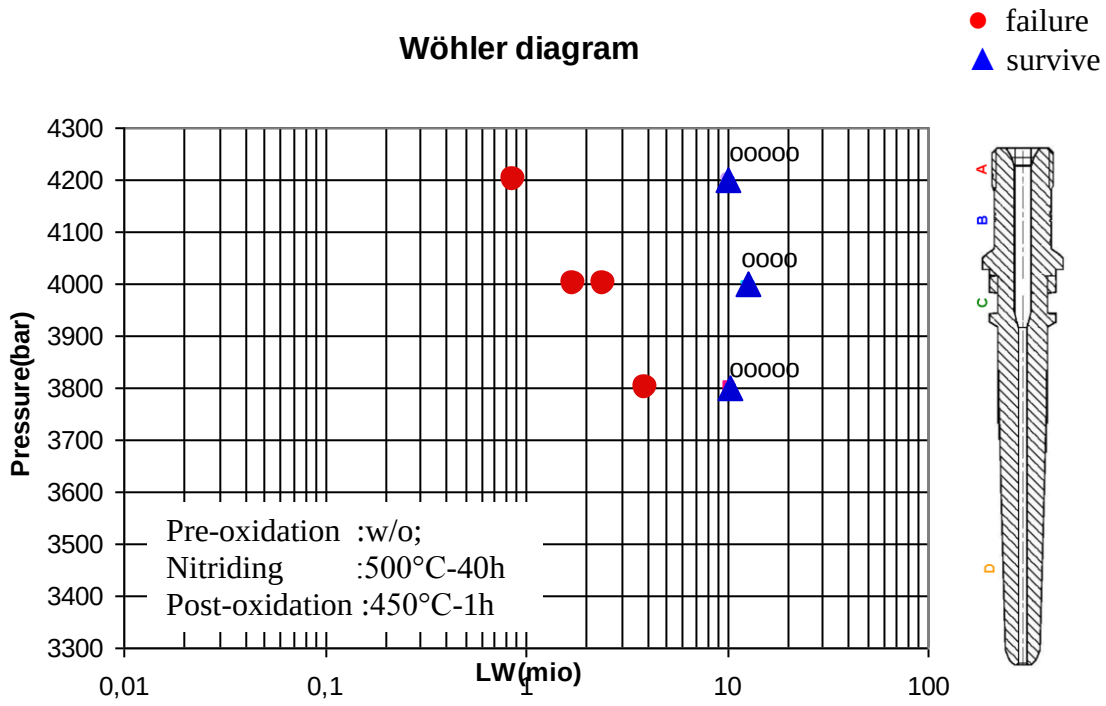

Figure 4.34 : Wöhler diagram of Trial 2 (Material:42CrMo4)

Three pressure levels were selected. The test was proceed until 10-12 million cycle. Six parts were tested for each pressure level. In the first pressure level (3800 bar) one part failed (red round) and five parts suvived (blue triangle). Two parts failed and four parts survived in the second pressure level (4000 bar). In the last pressure level (4200 bar) one part failed and five parts survived. Failure points were shown by red circles. There were calculated permitted pressure levels after pressure pulsation test. However, it was not possible to calculate the permitted pressure

because of scatter of the failed parts. Wöhler diagram can be seen for Trial 3 (520°C-6 h) which is short term nitriding duration in Figure 4.35 below. Number of parts and all analysis conditions and requirements are the same but there was extra pressure level which is 3600 bar to see minimum limit. Permitted pressure level was calculated as 2460 bar with safety factor 1.5.

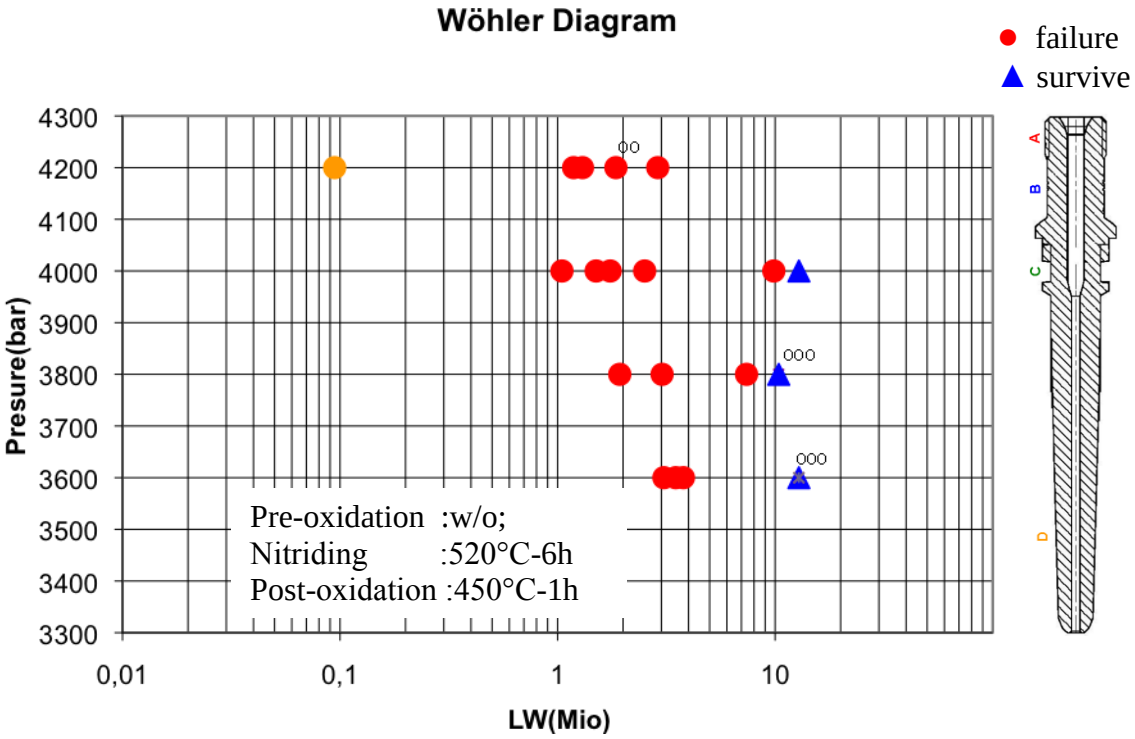

Figure 4.35 : Wöler diagram of Trial 3 (Material:42CrMo4)

4.5.3 Fracture analysis of high pressure connector

Fatigue strength was examined by pressure pulsation test. Afterward, failure analysis was investigated by SEM to see root causes of failures and crack initiation points. As seen from SEM image of samples from Trial 2 (Fig. 4.36), crack starts from hole on the high pressure component which is contact surface to filter catridge (Fig. 4.37). Crack starting point can be seen from SEM image (Fig. 4.38).

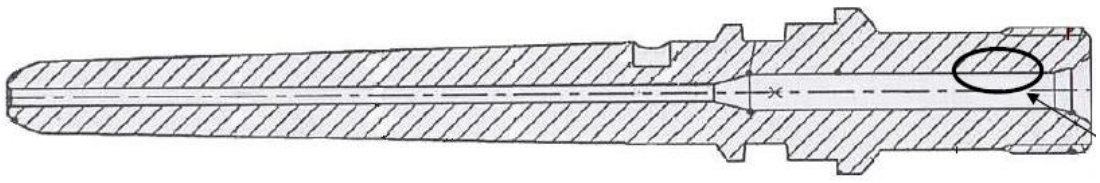

Figure 4.36 : Crack starting point of high pressure compenent for Trial 2 (500°C-(1+39)h)

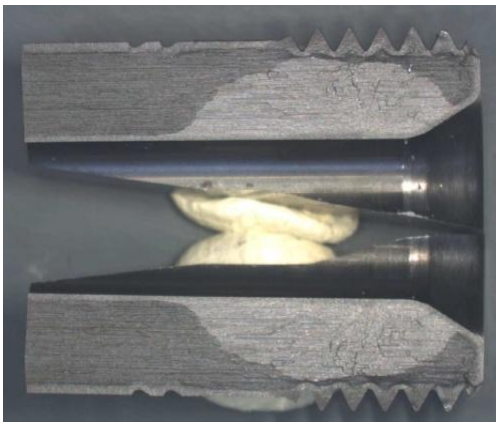

Figure 4.37 : Macro image of crack starting point

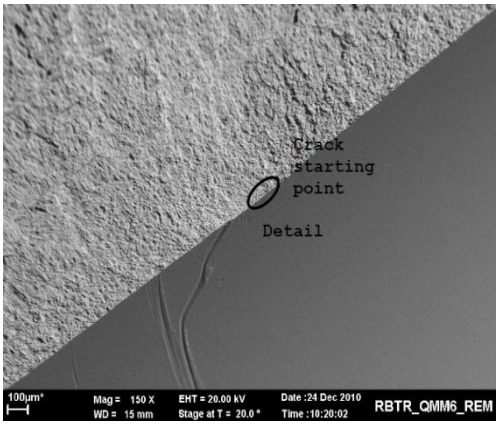

Figure 4.38 : SEM image of crack starting point (X150)

Failure points of Trial 3 (520°C-6 h) which is realtively short term nitriding can be seen from Figure 4.39. It was also cracked from filter connection point (A) but only one sample was cracked at the bottom side of the component(D) (Fig. 4.40).

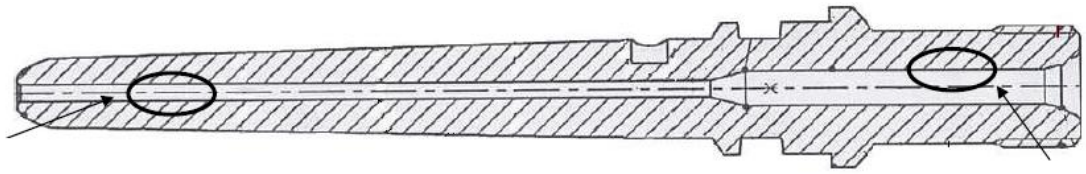

D **A**

Figure 4.39 : Crack starting point of high pressure compenent for Trial 3

Crack starting point (Fig. 4.41) and MnS inclusion (Fig. 4.42) in point of D can be seen below.

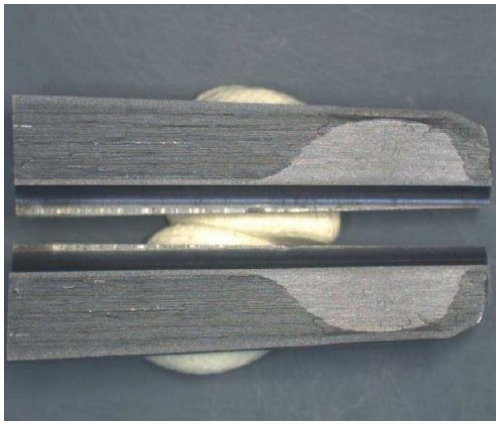

Figure 4.40 : Macro image of crack starting point (D)

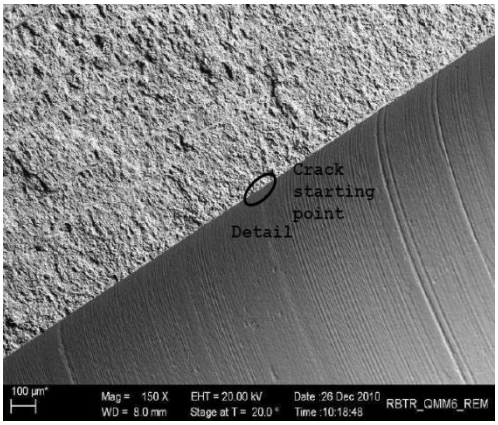

Figure 4.41 : SEM image of crack starting point (D) (X150)

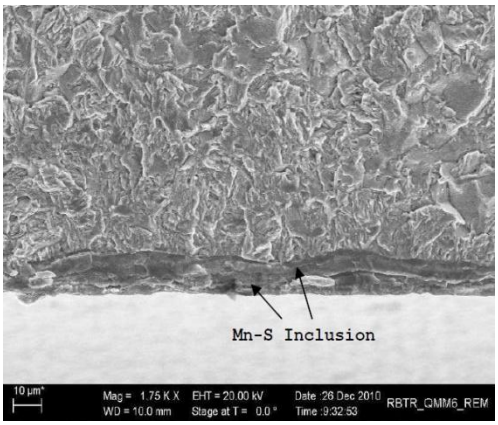

Figure 4.42 : SEM image of crack starting point (X1750)

4.5.4 Residual stress analysis of CR-injector

Residual stress behaviour of CR-Injector are shown in Figure 4.43 below. At the surface nitrided layer has less compressive residual stress. Along the nitriding depth firstly it increases and then decrease because of different nitrided precipitation mechanism [23].

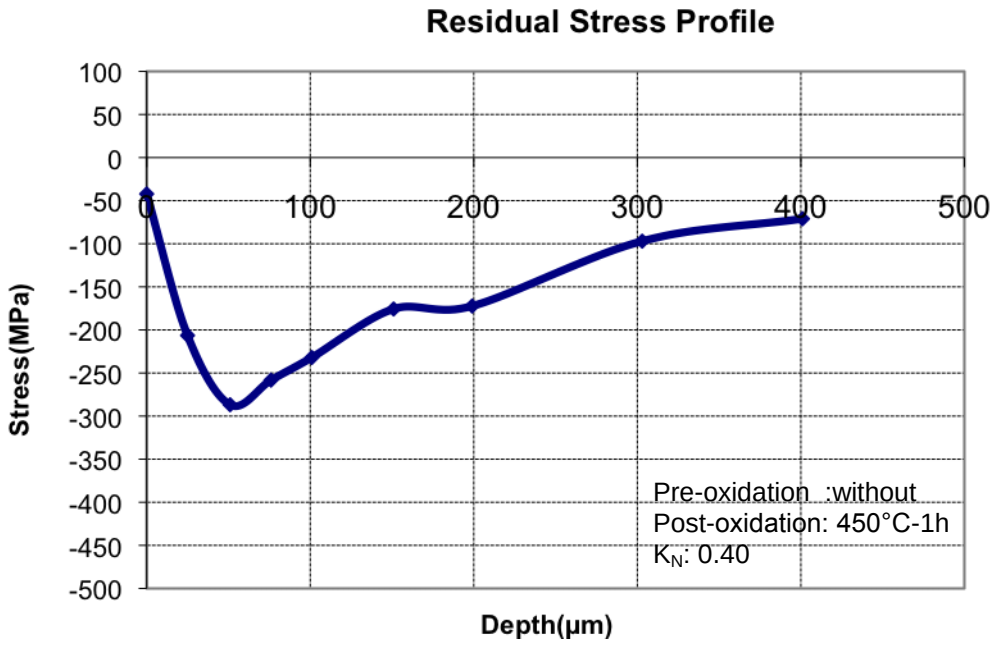

Figure 4.43 : Residual stress behaviour for CR-Injector (Material:50CrMo4)

4.5.5 Fatigue resistance of CR-injector

Fatigue strength tests were examined with same procedure with HPC. Pressure pulsation test for CR-Injector was examined for Trial 5 (520°C-6h). Wöhler diagram

can be seen in Figure 4.44 below. Loading pressure levels were selected as a 3600 and 4000 bar. Eight parts were loaded in pulsation test mechine for each pressure level. However all parts were failed at 4000 bar. Therefore, this pressure pulsation test was repeated by new nitriding trails with pasivating the crack surface where the all cracks were observed. The root cause was mentioned in Section 4.5.6. Wöhler diagram of repeated test is shown in Figure 4.45. Permitted pressure level for the repeated test was calculated as a 2550 bar with the safety factor 1.5.

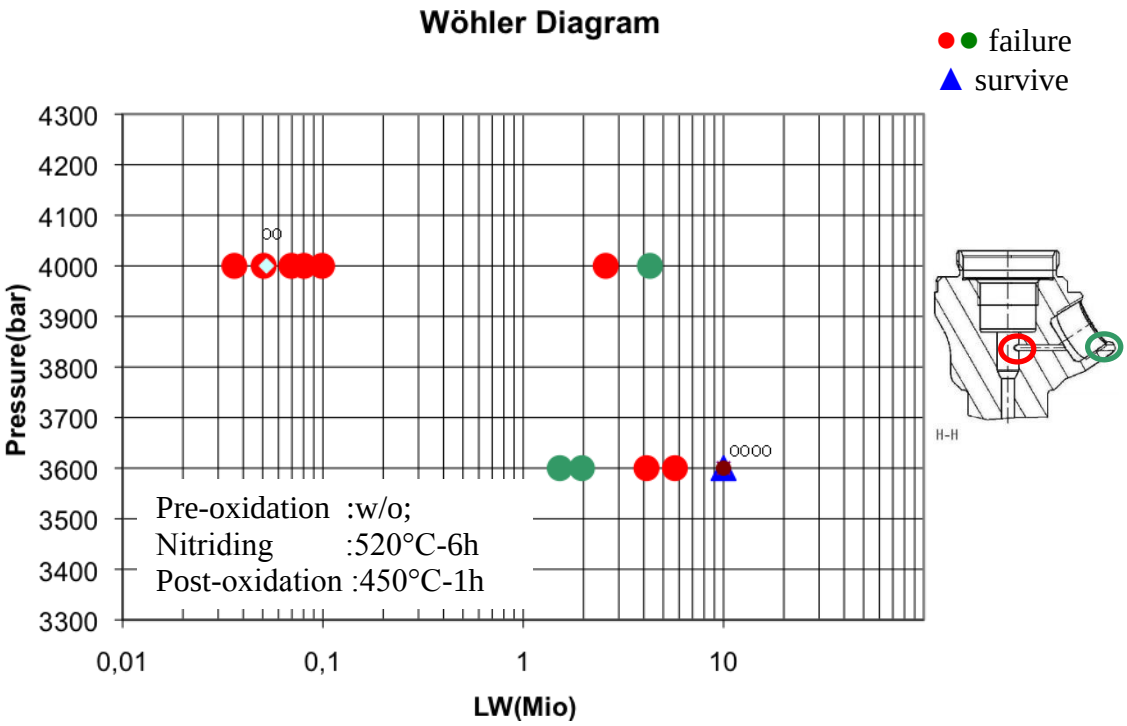

Figure 4.44: Wöler diagram of Trial 5 (Material:50CrMo4)

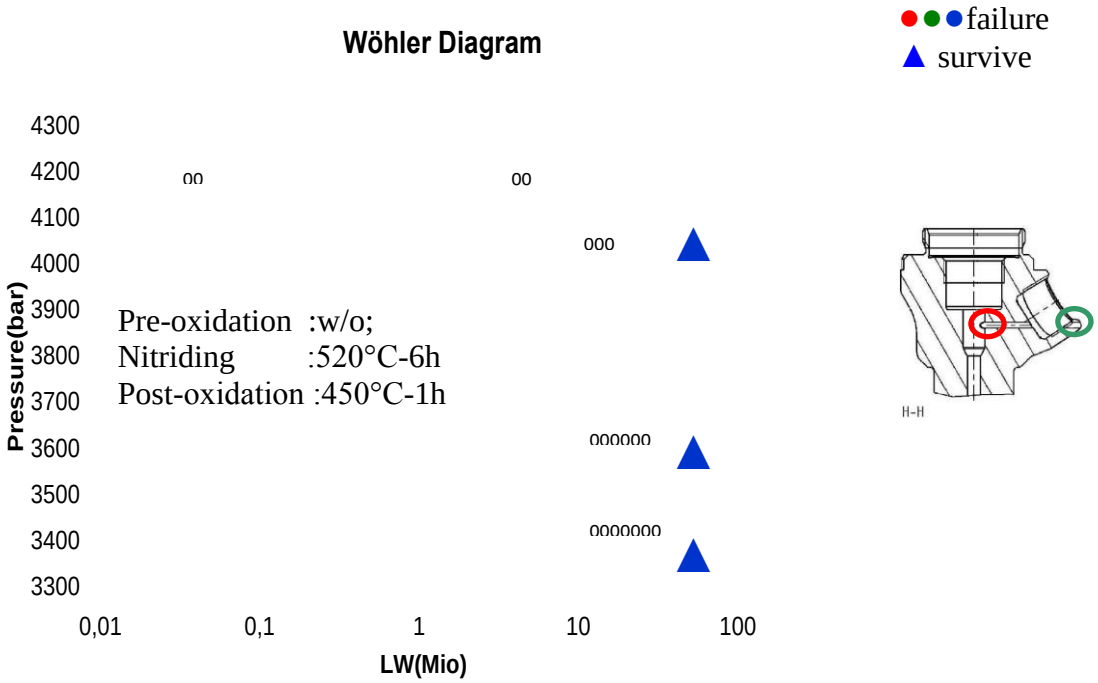

Figure 4.45 : Wöler diagram of Trial 5 (repeated) (Material:50CrMo4)

4.5.6 Fracture analysis of CR-injector

Failure analysis was also investigated for second trial series which were conducted by CR-Injectors. There was observed failure from three different points which are from seal surface (A), thread (B) and hole diameter decrease (C) for 520°C-(1+5) h (Fig. 4.46). Macro images of cracks can be seen in Figure 4.47

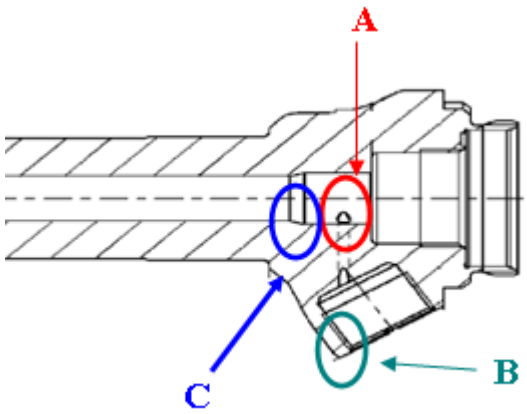

Figure 4.46 : Crack starting point of CR-injector for Trial 5

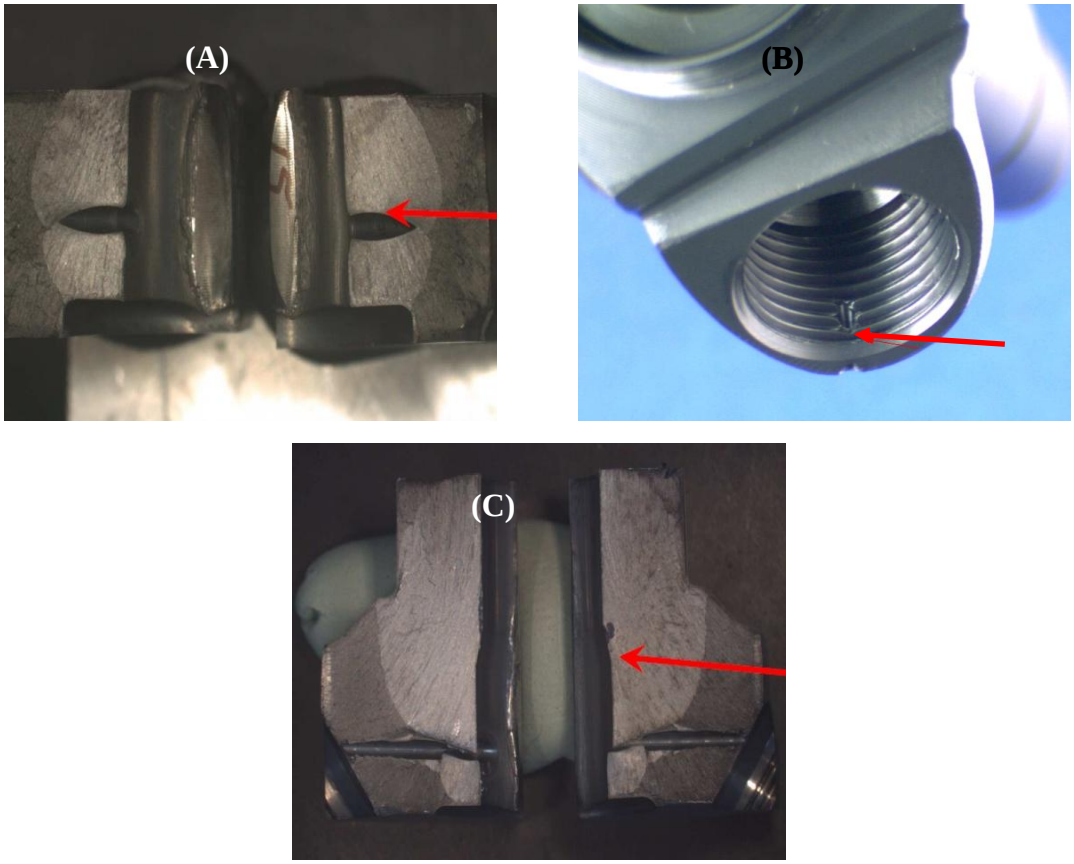

Figure 4.47 : Macro image of crack starting points from seal surface (A), thread (B) and hole diameter decrease (C)

The root cause of cracks, which are from Seal surface (A) and hole diameter decrease (C), are because of mean stress sensitivity. Root cause of another point (B) which is in the treads, is two directional nitriding inside of the hole. Therefore, this hole was closed by heat treatment pasting and repeated nitriding trial and pressure pulsation test. It was obtained more resist injector body as seen from Wöhler diagram (Fig. 4.44)

As a result of nitrided trails;

Four different nitriding trials were designed for HPC. It was observed temperature and time effect on fatigue strength. By increasing of temperature compound layer increased and also surface hardness increased. Relatively high temparture showed less compressive residual stress. Therefore, fatigue strenght decrease by increasing of temperature. Nitriding duration is also effected on fatigue strength. 1 hour unctrolled nitriding duration was used for each trial. By increasing of controlled

nitriding duration, both compound and diffusion layer thicknesses were also increased. At the same time, residual stress behaviour was changed along nitrided depth. Maximum compressive residual stress was gone to middle of the nitrided layer. Thus, surface near region had lower compressive residual stress than middle. Relatively long term nitriding (500°C-40h) showed better fatigue resistance. However, because of distortion, permitted pressure level was not calculated.

Common Rail Injectors were treated with 520°C and 6 hour. Residual stress measurements of both components showed different behaviour. However, permitted pressure levels were calculated very close.

Improvement of fatigue strength was achived until 2460 bar for inside of HPC that it is achieved until 2000 bar in the serial production by nitriding process which is 520°C, one hour uncontrolled nitriding duration and five hours controlled nitriding duration with K_N:0,40. Increasing of fatigue strength was succeed until 2550 bar for CR-Injector that it is achieved until 2000 bar in the serial production. However, fatigue strength needs to improve more and more for the next generation CR-Injector.

Crack initiation is effected of residual stress behaviour at surface near region. Thus, there should be maximum compressive residual stress in this region. They can be improved by nitriding recipitation mechanisim which depends on temperature, time and nitriding potential (Fig. 4.48).

Failure analysis shows that crack initiation starts from small regions which received two directional nitriding and diameter decreasing points. Therefore, these regions should be pasivated and also gas flow needs to be improved to overcome these problems.

After improvement of fatigue strength, pre and post oxidation treatments were designed to homogenize compound layer thickness and to increase corrosion resistance. Temperature and time effect were evaluated. It is obvious that all used pre-oxidation temperature and time increase homogenity of compound layer. However, pre-oxidation with 450°C and 1 hour and post-oxidation 450C 1 hour showed more stable compoud layer along the nitrided layer rom GDOES analysis (Fig. 4.25). In the corrosion test, the least Ri values were taken by post-oxidation with 450°C and 1 hour (Fig. 4.27). Beside the activation of hole component surface

pasivation also in the spesific regions like fuel discharge tube should be more improved to increse quality of components and to decrease crack initiations.

Post-oxidation treatments were determined to improve corrosion resistance comparison to phospating which is applied in serial production. All post-oxidation treatments achived less than Ri3. However, best result was taken by 450°C and one hour treatment with water.

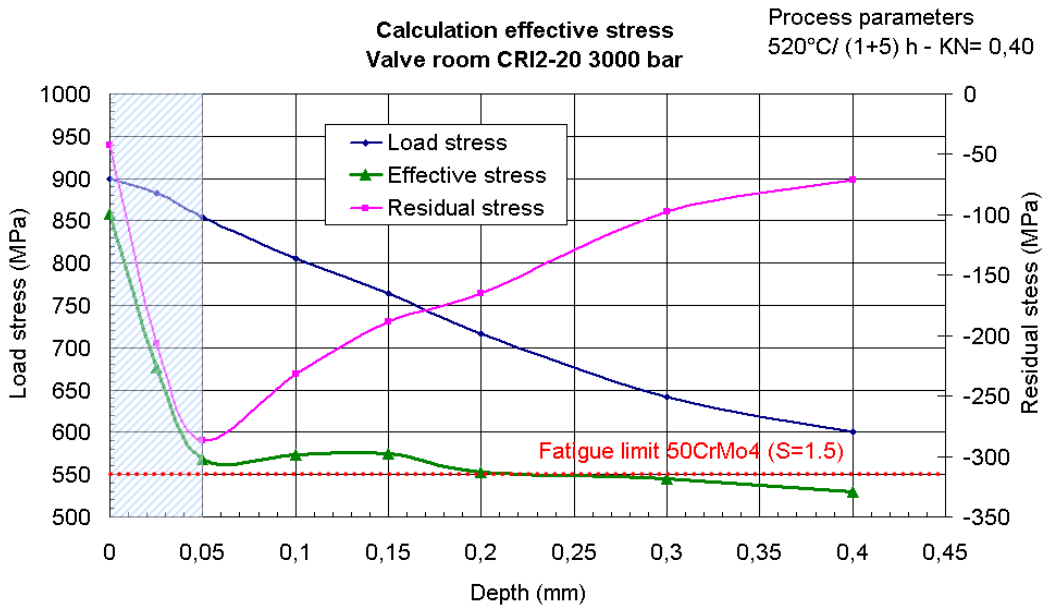

Figure 4.48 : Stress-depth profile of nitrided layer

5. CONCLUSION

Sensor controlled gas nitriding of tempered and quenched steels in the industrial furnace was achieved by both hydrogen and ammonia sensor which is designed by cooperation between Bosch in Turkey and Firma Stange in Germany. Nitriding temperatures were varied between 500°C and 520°C and nitriding duration between 6 and 40 hour with nitriding potantial 0,40.

There were aimed to increase fatigue strength for Diesel Injector components which are high pressure connectors and Common Rail Injectors. These components have different geometry and material composition. Therefore, the trails were examined for each component as a trials series. Nitriding at 520°C and 6 hours (1 hour uncontrolled, 5 hour controlled nitriding) were the best nitriding parameter for high pressure connector which permitted pressure level was calculated as a 2460 bar for fatigue stength. Second trial series were conducted with CR-Injectors. Nitriding parameters, which temperature was 520°C, nitriding duration was 6 hour (1 hour uncontrolled, 5 hour controlled nitriding), was chosen as a best parameter to permit pressure level as a 2550 bar.

Beside improving fatigue strength, high corrosion resistance was also aim of the thesis. There were examined pre-oxidation treatment with air to homogenize the compound layer thickness by activating the steel surface before nitriding. Pre-oxidation at 450°C and 1 hour was the best treatment parameter to homogenize CL thickness with high hardness. Compound layer should have not been so thick because it causes crack initiation. Therefore, there were investigated post treatment to increase corrosion resistance which is post-oxidation with water. Inside of the different post-oxidation parameter, there were chosen parameters, which post-oxidation temperature was 450°C and duration was 1 hour like pre-oxidation parameters. Both components were resisted until Ri3 salt spray test for 5,5 hour with these parameters.

By incresing the demands for diesel system, there should be investigated fatigue strength in nitriding process over 2500 bar. Therefore, there should be get tailor made nitrided layer for DI-Componenets. The demands can be achived by focusing cracks where is responsible of surface near region. Residual stress behaviour along the first 50 micrometer should be optimized by temperature and nitriding potantial.

All trails were done in the industrial furnace but it was used 40 parts for each trial in the same location to be comparible between trials. Therefore, there should be also investigated homogenity of the gas atmosphere from load to load and part top art to get high quality of the process.

As ssen from pulsation test results, some failures caused by more two directional diffusion mechanism esspecially small holes. Thus, pasivation of same regions are important as much as activation for the industry application.

Finally, the aim of the thesis, which was to get optimum nitriding parameters with pre and post treatments to increase fatigue strength and corrosion resistance, was got improvments. However, investigations will be go on to get more improvements for the industrial application.

REFERENCES

[1] **Bosch Internal Presentation**

[2] **C. H. Knerr, T.C. Rose, and J.H. Filkowski,** 1991: Gas Nitriding of Steels, Heat Treating, ASM Handbook, ASM International, Vol. **4**, p 387–409.

[3] **C. Hakan Gür, J. Pan,** 2009: Handbook of Thermal Process Modeling Of Steels, CRC Pres, Taylor & Francis.

[4] **D. Pye,** 2003: Practical Nitriding and ferritic nitrocarburizing, ASM International, Chapter 3, p 23-28

[5] **T. Greßmann,** 2007: Fe-C and Fe-N compound layers: Growth kinetics and microstructure, *PhD Thesis*, Stuttgart University-Max-Plank Institute, Stuttgart, Germany.

[6] **C. J. Weststrate,** 1979: Hydrocarbon And Ammonia Chemistry On Noble Metal Surfaces, *PhD Thesis*, Netherlands Institute of Catalysis, Netherlands.

[7] **url-1** <http://coursenotes.mcmaster.ca/701-702_Seminars/2005 2006/701_JeromeDarbellay_March_2006.pdf> accessed at 03.05.2011.

[8] **R. Pelka, W. Arabczyk**, 2009: Studies of the Kinetics of Reaction Between Iron Catalysts and Ammonia Nitriding of Nanocrystalline Iron with Paralel Catalytic Ammonia Decomposition, *Top Catal*, Vol. **52**, p 1506–1516.

[9] **A. Rainer Clauß,** 2008: Nitriding of Fe–Cr–Al alloys nitride precipitation and phase transformations, *PhD Thesis*, Stuttgart University-Max-Plank Institute, Stuttgart, Germany.

[10] **E. Lehrer,** 1930: Magnetic Investigation of the System Iron-Nitrogen, *Z. Electrochem*, Vol. **36**, p 383- 392.

[11] **S. S. Akhtar, A. F. M. Arif, Bekir Sami Yilbas,** 2010: Evaluation of gas nitriding process with in-process variation of nitriding potential for AISI H13 tool steel, *Int J Adv Manuf Technol*, Vol. **47**, p 687–698.

[12] **J. J. Braam, A. W. J. Gommers, S. Van Der Zwaag,** 1997: The influence of the nitriding temperature on the fatigue limit of 42CrMo4 and En40B steel, *Journal of Materials Science Letters*, Vol. **16**, 1327–1329.

[13] **N. Limodin, Y. Verreman,** 2003: T. N. Tarfa, Axial fatigue of a gas-nitrided quenched and tempered AISI 4140 steel:effect of nitriding depth, *Fatigue Fract Engng Mater Struct*, Vol. **26**, 811–820.

[14] **V.F. Terent'ev, M.S. Michugina, A.G. Kolmakov, V. Kvedaras, V. Čiuplys, A. Čiuplys, J. Vilys,** 2007: The effect of nitriding on fatigue strength of structural alloys, *Mechanica,* Vol. **64**, p 12-22.

[15] **B. Pennings, S. Van Der Zwaag,** 1998: The effect of metalworking fuids on the gas nitriding behavior of 31CrMoV9 steel, *Journal of Materials Science Letters,* Vol. **17**, p 1215-1217.

[16] **H. Sueyoshi, K. Hamaishi, S. Kadomatsu, T. Shiomizu, Y. Ohzono,** 1997: Effect of Preheating in Air on Gas Nitriding of SUS304 Stainless Steel, *Materials Trensactions,* Vol. **38**, p 148-154.

[17] **H. J. Spies, H. Le Thien, and H. B. Biermann,** 2004: Controlled Nitriding, Nitriding and Cabonitriding of Steel, *Metal Science and Heat Treatment,* Vol. **46**, p 7-11.

[18] **J. Michalski, J. Tacikowski, P. Wach, E. Lunarska, and H. Baum,** 2005: Formation of single-phase layer of γ'-Nitride in controlled gas nitriding, Chemicothermal Treatment, *Metal Science and Heat Treatment*, Vol. **47**, p 35-38.

[19] **E. K. Jeon, I. M. Park, I. Lee,** 2007: Plasma post-oxidation of nitrocarburized SUM 24L steel, *Materials Science and Engineering A,* Volumes **449-451**, p 868–871.

[20] **R. Sola, R. Giovanardi, P. Veronesi, G. Poli, S. Masini, A. Zanotti**, 2008: Development of Post-oxidation Treatments to Improve Wear and Corrosion Resistance, *la metallurgia italiana*, Vol. **3**, p 11-16

[21] M**. Bleeker, S. Gorter, S. Kersten, L. van der Ham, H. van den Berg, H. Veringa,** 2010: Hydrogen production from pyrolysis oil using the steam-iron process: a process design study, *Clean Techn Environ Policy,* Vol. **12**, p 125–135.

[22] **N. Mandkarian, F. Mahboubi,** 2009: Effect of gas mixture of plasma post-oxidation on corrosion properties of plasma nitrocarburised AISI 4130 steel, *Vacuum,* Vol. **83**, p 1036–1042.

[23] **N. E. Vives Dı´az , R. E. Schacherl, L. F. Zagonel, E. J. Mittemeijer,** 2008: Influence of the microstructure on the residual stresses of nitrided iron-chromium alloys, *Acta Materialia*, Vol. **56**, p 1196–1208.

[24] **ASTM B117**, 2009. Standard Practice for Operating Salt Spray (Fog) Apparatus, *American Society for Testing and Materials (ASTM) International Standards,* USA.

[25] **DIN EN ISO 9227**, 2006. Corrosion tests in artificial atmospheres - Salt spray tests, *Europeon Standards,* Germany.

[26] **EN ISO 4628-3**, 2003. Assessment of degree of rusting, *Europeon Standards*, Germany.

CURRICULUM VITAE

Candidate's full name **:** Zühre Varol

Place and date of birth **:** Bursa 17.05.1986

Permanent Address **:** Beşevler-Nilüfer/Bursa

Universities and Colleges attended **:**

2000-2004 Bursa Boys' High School

2004-2009 Ankara University-Chemical Engineering

2009- 2011 İstanbul Technical University-Material Science and Engineering.